Palaeogeography, Palaeoclimatology, Palaeoecology 592 (2022) 110909

Contents lists available at ScienceDirect

Palaeogeography, Palaeoclimatology, Palaeoecology

journal homepage: www.elsevier.com/locate/palaeo

# Preservation and diagenesis of soft-bodied fossils and the occurrence of phosphate-associated rare earth elements in the Cambrian (Wuliuan) Spence Shale Lagerstätte

Anna F. Whitaker [a,*], James D. Schiffbauer [b,c], Derek E.G. Briggs [d], Wade W. Leibach [b,c], Julien Kimmig [e,f]

[a] Department of Chemical and Physical Sciences, University of Toronto Mississauga, 3359 Mississauga Road, Mississauga, ON L5L 1C6, Canada
[b] Department of Geological Sciences, University of Missouri, Columbia, MO 65211, USA
[c] X-Ray Microanalysis Core, University of Missouri, Columbia, MO 65211, USA
[d] Department of Earth and Planetary Sciences, and Yale Peabody Museum of Natural History, Yale University, New Haven, CT 06520, USA
[e] Department of Geosciences, Pennsylvania State University, University Park, PA 16802, USA
[f] Earth and Environmental Systems Institute, Pennsylvania State University, University Park, PA 16802, USA

ARTICLE INFO

Editor: Dr. Howard Falcon-Lang

*Keywords:*
Lagerstätte
Taphonomy
SEM-EDS
Burgess Shale-type preservation
Great Basin

ABSTRACT

The Spence Shale Lagerstätte is a middle Cambrian (Miaolingian Series; Wuliuan Stage) fossil deposit in northern Utah and southern Idaho, USA. At present, it is known to preserve 89 species, from at least 10 phyla, of biomineralizing and soft-bodied taxa, and represents the only major Lagerstätte of Wuliuan age in Laurentia outside the Canadian Rockies. In addition to taxonomic diversity, the Spence Shale exposures represent a variety of depositional environments along a continental shelf, which have been affected by several diagenetic events, making it a compelling setting to improve our understanding of taphonomic and diagenetic pathways as they affect the broader Burgess Shale-type (BST) preservation. We present analyses of 28 specimens from six localities using scanning electron microscopy (SEM) and integrated energy dispersive X-ray spectrometry (EDS), together with comparisons of published data. Taxa are predominantly preserved as a combination of carbonaceous compressions, iron oxide and pyrite replacement, but eldoniids of the genus *Eldonia* consistently show enrichment in rare earth elements (REE). The REE, predominantly lanthanum and cerium, are enriched in the phosphate mineral monazite, which occurs in the inner coil of *Eldonia ludwigi*. This pattern, seen in all sampled *Eldonia*, differs from previous reports of REE association in BST preservation in being limited to one tissue type within a specific identifiable taxon. REE enrichment of tissues can occur during the lifetime of an individual or during fossilization, and we present both possible pathways along with an outline of taphonomic processes leading to the preservation of soft-bodied fossils from the Spence Shale.

## 1. Introduction

The Spence Shale Lagerstätte (referred to as Spence Shale from here on) is a middle Cambrian (Miaolingian Series, Wuliuan Stage) Burgess Shale-type (BST) Lagerstätte that has recently been the center of renewed attention for its taxonomic diversity and complex preservation. Located in northern Utah and southern Idaho, U.S.A., it is the oldest of the five Utah Cambrian BST Lagerstätten (Kimmig et al., 2019) and the only one located outside the House Range and Drum Mountains (Robison et al., 2015; Lerosey-Aubril et al., 2018; Kimmig et al., 2019). The fauna of the Spence Shale comprises a diverse community of, in order of generic abundance, trilobites, soft-bodied arthropods, brachiopods, echinoderms, molluscs, sponges, lophophorates, scalidophorans, hemichordates, lobopodians, algae, potential cyanobacteria, and multiple problematic taxa (e.g., *Banffia*, *Eldonia*, and *Siphusauctum*) (Kimmig et al., 2019). In recent years, numerous new taxa from the Spence Shale have been described and several additional taxa have been revised, bringing the faunal diversity to at least 89 species in 74 genera (e.g., Legg and Pates, 2017; Kimmig et al., 2017; Pates et al., 2018; Wen et al., 2019; Sundberg, 2020; Whitaker et al., 2020; Kimmig and Selden,

* Corresponding author.
*E-mail addresses:* a.whitaker@mail.utoronto.ca (A.F. Whitaker), schiffbauerj@missouri.edu (J.D. Schiffbauer), derek.briggs@yale.edu (D.E.G. Briggs), wade.leibach@gmail.com (W.W. Leibach), jkimmig@gmail.com (J. Kimmig).

https://doi.org/10.1016/j.palaeo.2022.110909
Received 9 October 2021; Received in revised form 26 February 2022; Accepted 1 March 2022
Available online 4 March 2022
0031-0182/

2021). This makes the Spence Shale one of the most diverse BST deposits (e.g., Kimmig et al., 2019; Nanglu et al., 2020; Yang et al., 2021a). The depositional conditions of the Spence Shale have been investigated, revealing rapid fluctuations from oxic to dysoxic benthic environments and moderate bioturbation (Garson et al., 2012; Kloss et al., 2015). However, investigations of the taphonomy of the member have been limited to broad overviews or specific taxonomic groups, further restricted by sampling from just a few localities. Gaines et al. (2008) reported the prevalence of carbonaceous films as evidence of a common taphonomic pathway among BST deposits, and Broce and Schiffbauer (2017) documented variation in the preservation pathways of vermiform fossils, including kerogenization, pyritization, aluminosilicification, and phosphatization. Broce and Schiffbauer's (2017) samples of Spence Shale fossils, however, only included examples from the Wellsville Mountains (Fig. 1). The Wellsville localities have yielded the majority of soft-bodied fossils from the Spence Shale and the greatest

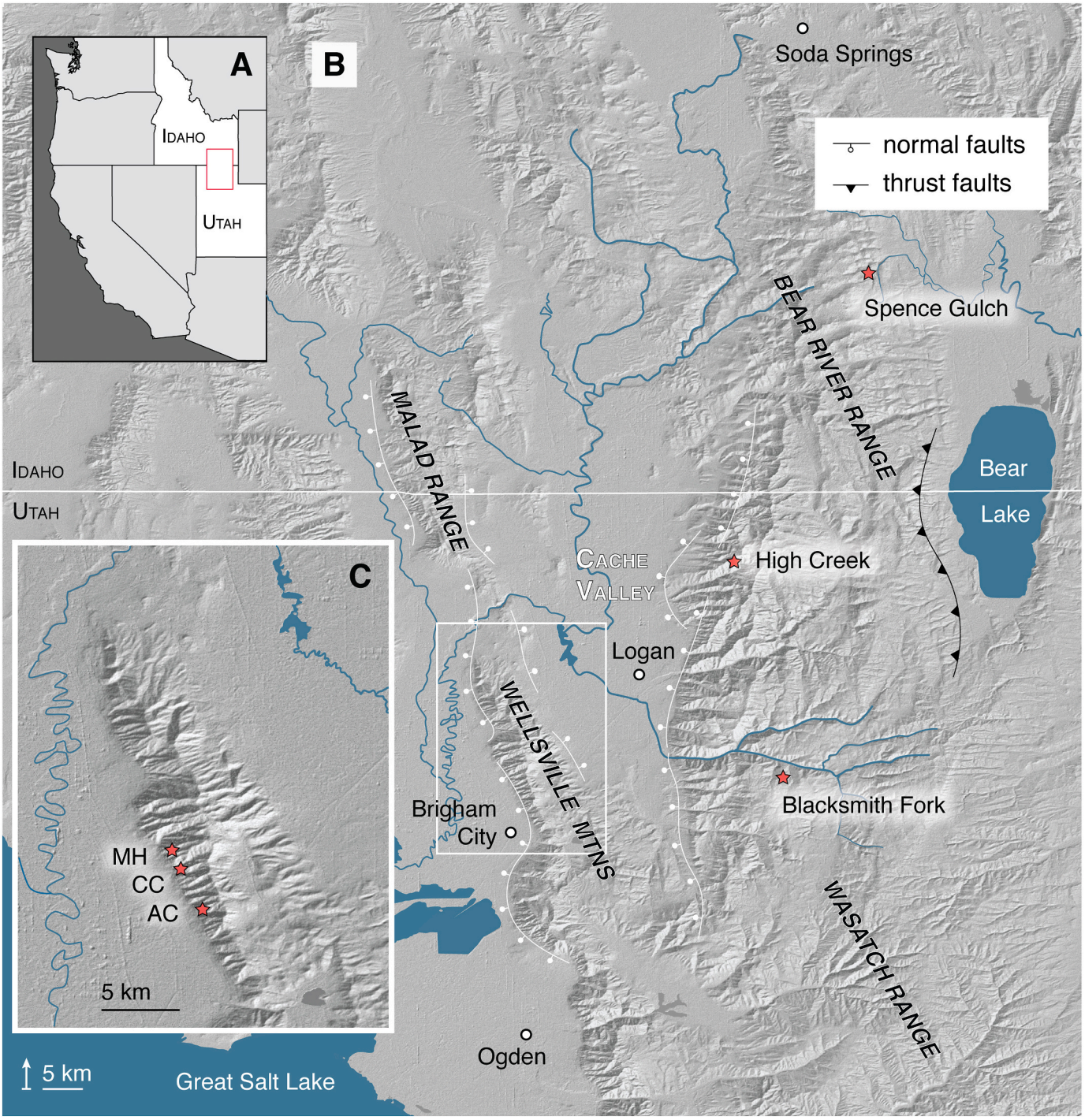


**Fig. 1.** Location and localities of the Spence Shale Lagerstätte. A) Map of the western United States of America showing location of the Spence Shale. B) Relief map of northern Utah and southern Idaho showing prominent localities and geologic features relating to the Spence Shale. C) Close-up of inset from (B), showing position of localities within the Wellsville Mountains. MH, Miners Hollow; CC, Cataract Canyon; and AC, Antimony Canyon. Study sites are protected, but exact location information will be shared with qualified researchers upon request. We acknowledge the use of imagery from the NASA Worldview application (https://worldview.earthdata.nasa.gov), part of the NASA Earth Observing System Data and Information System (EOSDIS).

diversity (Kimmig et al., 2019; Whitaker and Kimmig, 2020), but the taxonomic distributions and taphonomic conditions at other Spence Shale localities can offer new insights.

The Spence Shale differs from many other BST Lagerstätten in the preservation of depositional environments varying from shallow shelf carbonates to deeper water shales (Kimmig et al., 2019). This environmental range, as well as the occurrence of soft-tissue preservation at multiple stratigraphic horizons within exposures, makes the Spence Shale ideal for the investigation of taphonomic response to different settings. Our analyses using scanning electron microscopy (SEM) and integrated energy dispersive X-ray spectrometry (EDS) offer insights into the initial stages of fossil preservation and subsequent diagenetic history at different Spence Shale localities, their impact on the taphonomy of soft-tissues, and the importance of understanding these processes across BST Lagerstätten.

## 2. Geologic Context

The Spence Shale crops out in northern Utah and southern Idaho at multiple exposures in the Wellsville Mountains, the Bear River Range, the Wasatch Range, and the Malad Range (Fig. 1). The Spence Shale is the middle member of the Langston Formation, conformably overlying the Naomi Peak Limestone Member and underlying the High Creek Limestone Member at the type locality in Spence Gulch. The Langston Formation (type locality: Blacksmith Fork) conformably overlies the Geersten Canyon Quartzite and is in turn conformably overlain by the Ute Formation (Walcott, 1908; Kimmig et al., 2019). The Spence Shale straddles the *Albertella* to *Glossopleura* trilobite biozones, and is therefore slightly older than the Burgess Shale in Canada (Kimmig et al., 2019). It has been interpreted as representing deposition in the middle to outer detrital belt of a (presently) westward-oriented carbonate platform (Robison, 1991; Liddell et al., 1997). There is an overall proximal to distal trend towards the NE, with extensive soft-tissue preservation and dolomitization in the Wellsville Mountain localities, which decrease in the Bear River and Malad Range localities (Kimmig et al., 2019).

The Langston Formation has undergone extensive dolomitization, which extends into the Spence Shale (Deiss, 1938; Whitaker et al., 2020). The timing of this dolomitization has been interpreted as eogenetic to mesogenetic, and controlled largely by facies, correlating strongly with the upper peritidal deposits under a seepage reflux model (Butterbaugh, 1982). However, this model does not account for the significant dolomitization of the Spence Shale Member.

The Wasatch Range is approximately centered in the Sevier Wyoming-Idaho-Utah thrust belt, formed by the Servier and Laramide orogenies. The Paris thrust fault, which runs roughly north-south on the eastern side of the Bear River Range (Valenti, 1982), creates a 3600 ft stratigraphic displacement, placing the Langston Formation in contact with the Furongian St. Charles Formation in the Laketown Quadrangle (Valenti, 1982).

The Utah Basin and Range extension, beginning 17 mya, formed the modern topography of the Spence Shale outcrops. These features are high-angle normal faults, creating the horst block mountain ranges and fault scarps enclosing the Cache Valley, a half-graben basin (Williams, 1948; Evans and Oaks Jr., 1996; Black et al., 2000). The relevant faults are the East Cache Fault zone, the West Cache Fault zone, and the Wasatch Fault (McCalpin, 1994; Black et al., 2000). These faults remain active to the present, with multiple seismic events in the sub-recent record (McCalpin, 1994).

The Bonneville lake cycle began approximately 30 kya, and periodically rose and fell, filling the Cache Valley. The Bonneville Shoreline level (18,000 B.P.) represents the highest paleo-shoreline (Hylland, 2007) but, as reconstructed by Chen and Maloof (2017), it does not affect known localities of the Spence Shale.

## 3. Material and methods

Twenty-eight specimens representing 6 localities were analyzed using scanning electron microscopy (SEM) and integrated energy dispersive X-ray spectrometry (EDS): from Antimony Canyon ($n = 8$), Blacksmith Fork ($n = 1$), Cataract Canyon ($n = 3$), High Creek ($n = 2$), Miners Hollow ($n = 9$), and Spence Gulch ($n = 5$) (Table 1). Samples were selected from the University of Kansas Invertebrate Paleontology collections based on generic occurrence at multiple localities, and the availability of stratigraphic data. Specimens represent at least 6 phyla (Lobopodia, Arthropoda, Lophotrochozoa, Mollusca, Priapulida, Hemichordata) as well as problematic taxa. An additional 18 specimens from previous studies (Marshall et al., 2012; LoDuca et al., 2015; Broce and Schiffbauer, 2017; Whitaker et al., 2020; Kimmig and Selden, 2021; Moon et al., 2021) were added to the dataset, giving a total of 46 specimens (Table 1). Genera represented are *Acinocricus, Anomalocaris, Armilimax, Dioxycaris, Eldonia, Hurdia, Isoxys, Mollisonia, Selkirkia, Sphenoecium, Utahscolex, Waptia, Wiwaxia,* along with unidentified hurdiids, vermiform taxa, and bradoriids (Table 1). The specimens represent a range of tissue types, including cellular, cuticularized and sclerotized, and multiple tissue types are often present within a specimen. Selection within a genus was determined by which individuals preserve the most tissue types. Specimens were photographed immersed in alcohol (except where noted) using a Leica DMS 300 Digital Microscope and an Olympus SZX16 microscope. Whole specimen images were created by stitching together mosaics of smaller images using Adobe Photoshop. Specimens too large for microscope photography were photographed using a Pentax K-5 SLR digital camera, and image settings were adjusted in Adobe Photoshop.

SEM imaging of KUMIP 204390 and KUMIP 314041 was conducted using an FEI Versa 3D Dual Beam FIB-SEM (focused ion beam not used, electron imaging only) at the University of Kansas Microscopy and Analytical Imaging Laboratory. EDS analysis of KUMIP 204390 was conducted using an Oxford Instruments 80 $mm^2$ x-Max silicon drift detector. Analyses conducted on this instrument used an accelerating voltage of 10 keV and a spot size of 4.5, under low vacuum conditions.

SEM and EDS analyses of KUMIP 312404 and KUMIP 314037 were conducted using a Philips XL 30 environmental scanning electron microscope (ESEM) with a Princeton Gamma-Tech EDS at Yale University; images were generated at 10 keV with a spot size of 3 (roughly 2 nm in diameter) at a working distance ~10 mm.

SEM-EDS imaging for all the other samples in the present study was conducted at the X-ray Microanalysis Core Facility at the University of Missouri, using a Zeiss Sigma 500 VP variable pressure SEM with dual, co-planar Bruker XFlash 6|30 EDS detectors (30 $mm^2$). Analyses conducted on this instrument used the following operating conditions, with minor variation: beam accelerating voltage of 20 keV and current of 40 nA, a 60 μm aperture for imaging and a 120 μm aperture for EDS analyses, a working distance of 16 mm ± 2 mm, and a chamber vacuum of 25 ± 5 Pa.

Conditions used in previous studies are reported in the respective publications. All elements detected were mapped. Maps of prominent elements are included in figures, and all maps of all specimens are included in Appendix 1.

Saleh et al. (2020a) compared the taphonomic signals of three exceptionally preserved biotas (the Burgess Shale, the Chengjiang Biota, and the Ordovician Fezouata Shale) using the presence and co-occurrences of five tissue types. Using their approach and dataset, we added data compiled herein from the Spence Shale samples for comparison (Appendix B), evaluating each eumetazoan genus for the presence of a biomineralized skeleton, sclerotized tissue (i.e. possessing an organically strengthened part or organ), unsclerotized cuticle (i.e. a non-cellular outer body surface that is either collagenous or formed by polymerized polysaccharides), soft cellular outer layer defining at least a part of the body (e.g. hyolith tentacles), and soft internal cellular organ/tissue (e.g. digestive or nervous systems) (Saleh et al., 2020a).

**Table 1**
Details of specimens analyzed in this study and previously published information.

| Specimen # | Taxonomic Designation | Description | Study reference | Locality | Stratigraphic Info | Preservation |
|---|---|---|---|---|---|---|
| KUMIP 563151 | *Selkirkia* | Tube | this study | Cataract Canyon | Float | Aluminosilification |
| KUMIP 563145 | *Selkirkia* | Tube | this study | High Creek | n/a | Iron-association/pyrite |
| KUMIP 563150 | *Selkirkia* | Tube | this study | Spence Gulch | n/a | Iron-association/pyrite |
| KUMIP 314158 | *Selkirkia spencei* | Tube | this study | Miners Hollow | n/a | Iron-association/pyrite |
| KUMIP 144845 | *Selkirkia spencei* | Tube | this study | Antimony Canyon (S side) | Gunther Quarry 3 to 5 m below top (in situ) | Kerogenization; Iron-association/pyrite |
| KUMIP 558518 | *Dioxycaris* | Isolated Carapace | this study | Spence Gulch | n/a | Kerogenization; Iron-association/pyrite |
| KUMIP 135145 | *Dioxycaris argenta* | Isolated Carapace | this study | Antimony Canyon (S side) | About 3 m below top of Spence Tongue | Kerogenization; Iron-association/pyrite |
| KUMIP 579390 | Bradoriida | Shell | this study | Spence Gulch | 5 m in situ | Calcium association, Kerogenization; Iron-association/pyrite |
| KUMIP 514259 | *Sphenoecium wheelerensis* | Branching tubes | this study | Antimony Canyon | n/a | Kerogenization; Iron-association/pyrite |
| KUMIP 495314 | *Sphenoecium wheelerensis* | Branching tubes | this study | Miners Hollow | Upper Cycle 3 - Koot. Quarry (in situ) | Kerogenization; Iron-association/pyrite |
| KUMIP 514260 | *Sphenoecium wheelerensis* | Branching tubes | this study | High Creek | n/a | Iron-association/pyrite |
| KUMIP 490937 | *Eldonia* | concentrated debris around degraded body | this study | Cataract Canyon | Float | REE-enriched phosphatization, Kerogenization |
| KUMIP 204370 | *Eldonia ludwigi* | Soft tissue body with gut | this study | Antimony Canyon (S side) | 3 to 5 m below top (ecavated, likely) | REE-enriched phosphatization, Kerogenization |
| KUMIP 510274–510275 | *Eldonia ludwigi* | Soft tissue body with gut | this study | Miners Hollow | Upper Cycle 3 - float | REE-enriched phosphatization, Kerogenization |
| KUMIP 204366 | *Wiwaxia* | Isolated spine | this study | Antimony Canyon (S side) | 3 to 5 m below top | Kerogenization; Iron-association/pyrite |
| KUMIP 490944 | *Wiwaxia* | Isolated spine | this study | Miners Hollow | Upper Cycle 3 - Koot. Quarry (in situ) | Kerogenization; Iron-association/pyrite |
| KUMIP 490967 | *Acinocricus stichus* | Isolated spines | this study | Antimony Canyon | Float | Aluminosilification |
| KUMIP 491082 | *Acinocricus stichus* | Isolated spines | this study | Cataract Canyon | Float | Iron-association/pyrite |
| KUMIP 314131 | *Acinocricus stichus* | Isolated spines | this study | Miners Hollow | n/a | Calcium association; Iron-association/pyrite |
| KUMIP 491056 | *Hurdiidae* | Feeding appendage | this study | Miners Hollow | Lower Cycle 6, 155′ (in situ) | Kerogenization; Iron-association/pyrite; Calcium association |
| KUMIP 491057 | *Hurdiidae* | Isolated Carapace | this study | Antimony Canyon | Float | Kerogenization; Iron-association/pyrite; Calcium association |
| KUMIP 314056 | *Hurdia victoria* | Isolated Carapace | this study | Miners Hollow | Cycle 3; 130 ft. above base | Kerogenization; Iron-association/pyrite |
| KUMIP 204779 | *Sidneyia?* | Feeding appendage | this study | Miners Hollow | Upper | Aluminosilification; Iron-association/pyrite |
| KUMIP 204777 | *Sidneyia?* | Feeding appendage | this study | Antimony Canyon | n/a | Kerogenization; Iron-association/pyrite |
| KUMIP 579391 | Bradoriida | Shell | this study | Spence Gulch | 1 m (in situ) | Kerogenization; Calcum phosphate |
| KUMIP 557975 | Vermiform | Possible body fossil with gut(?) | this study | Spence Gulch | (in situ) | Aluminosilification; Iron-association/pyrite |
| USNM 768408 | *Selkirkia* | Tube | this study | Blacksmith Fork**Possibly Ute Fm. (Deiss, 1938) | n/a | Kerogenization; Iron-association/pyrite |
| KUMIP 314041 | *Mollisonia symmetrica* | Articulated body fossil | this study | Miners Hollow | Cycle 3; ~130′ above base of Spence Shale | Kerogenization |
| KUMIP 312404 | *Isoxys* | Carapace with eye and traces of appendages | this study (previously unpublished data) | Miners Hollow | mid? | Iron-association/pyrite |
| KUMIP 314037 | *Anomalocaris* | Articulated body fossil, with mouthparts and appendages, nearly complete | this study (previously unpublished data) | Miners Hollow | n/a | Pyrite, phosphatization of muscle near gut |
| KUMIP 490943 | *Armilimax pauljamisoni* | Articulated body fossil, soft tissue with shell and gut tract, | Kimmig and Selden, 2021 | Miners Hollow | Cycle 3; ~33–36 m above base (as measured by Kimmig) | Phospatization in shell, minor phosphatization in soft tissue, Kerogenization |
| KUMIP 204390 / UMNH IP 4696 | *Utahscolex ratcliffei* | Articulated body fossil with gut tract, missing anterior/posterior termination | Whitaker et al., 2020 | Miners Hollow | Cycle 3, float | Iron-association/pyrite |
| KUMIP 490902 | *Utahscolex ratcliffei* | | Whitaker et al., 2020 | Miners Hollow | Cycle 3, float | Calcium phosphate (plates); Aluminosilification |

(*continued on next page*)

**Table 1** (*continued*)

| Specimen # | Taxonomic Designation | Description | Study reference | Locality | Stratigraphic Info | Preservation |
|---|---|---|---|---|---|---|
| | | Articulated body fossil with gut tract, missing posterior termination | | | | |
| KUMIP 314107 | Animalia, unknown | Body fossil? | Broce and Schiffbauer, 2017 | Miners Hollow | n/a | Phosphatized |
| KUMIP 314111 | Annelida? | Body fossil? | Broce and Schiffbauer, 2017 | Miners Hollow | Cycle 3; 130 ft. above base | Kerogenization, pyrite associated aluminosilification, bladed barite |
| KUMIP 314112 | Ichnofossil, *Planolites*? | | Broce and Schiffbauer, 2017 | Miners Hollow | n/a | Pyrite |
| KUMIP 314114 | Animalia, unknown | Body fossil? | Broce and Schiffbauer, 2017 | Antimony Canyon | "middle" spence shale | Pyrite and monazite associations |
| KUMIP 314159 | Animalia, unknown | Body fossil? | Broce and Schiffbauer, 2017 | Miners Hollow | n/a | Pyrite |
| KUMIP 314186 | Animalia, unknown | Body fossil? | Broce and Schiffbauer, 2017 | Miners Hollow | Cycle 6; 160 ft. level | Kerogenization, pyrite-association, aluminosilification, monazite, calcite |
| KUMIP 314191 | Animalia, unknown | Body fossil? | Broce and Schiffbauer, 2017 | Miners Hollow | 2/3 down from top | Pyrite and barite association |
| KUMIP 314202 | Ichnofossil | | Broce and Schiffbauer, 2017 | Miners Hollow | n/a | Pyrite |
| KUMIP 314215 | *Annelida?* | Body fossil? | Broce and Schiffbauer, 2017 | Wellsville Mtn. | n/a | Pyrite and barite |
| KUMIP 377069 | Ichnofossil | | Broce and Schiffbauer, 2017 | Miners Hollow | n/a | Iron-association/pyrite |
| KUMIP 314270 | *Sphenoecium wheelerensis* | Specimen with multiple tubes | LoDuca et al., 2015 | Wellsville Mtn. | ~10 ft. below top | Iron-association/pyrite |
| KUMIP 314028 | *Leanchoilia superlata* | Body fossil | Marshall et al., 2012 | Miners Hollow | n/a | Iron-association/pyrite |
| KUMIP 314032 | *Waptia* cf. *fieldensis* | Body fossil with gut tract and eggs | Moon et al., 2021 | Miners Hollow | n/a | Phosphatized (eggs) |

Institutional abbreviations: KUMIP, Division of Invertebrate Paleontology, Biodiversity Institute, University of Kansas, Lawrence, KS, USA; USNM PAL, Paleobiology Department, Smithsonian National Museum of Natural History, Washington, D.C., USA; UMNH IP, Natural History Museum of Utah, Salt Lake City, UT, USA.

## 4. Results

The specimens from the Spence Shale show a variety of preservation modes but are predominantly preserved as kerogenized/carbonaceous compressions, pyrite framboids, and weathered iron oxides. A full summary of specimen preservation is provided in Table 1; all EDS elemental maps are included in Appendix A. Soft-tissue preservation occurs in at least three sequences at Miners Hollow, within the Cycle 3 and Cycle 6 intervals (MH3L, MH3U of Cycle 3, and MH6 of Cycle 6, of Garson et al., 2012). Samples from these intervals show that MH3L is mainly non-bioturbated, MH3U is weakly bioturbated, and MH6 shows variations in bioturbation. As documented previously, bioturbation increases up-section within each cycle (Garson et al., 2012). Cycle 3 contains fossils preserved via carbonaceous compressions ($n = 7$), iron mineral associations ($n = 5$), phosphatization ($n = 2$), aluminosilification (n = 2), and phosphatization enriched with REEs (hereafter, REE-associated phosphatization; $n = 1$)\ (Table 1). Cycle 6 contains iron associations (n = 2), carbonaceous compressions (n = 2), calcium association (n = 2), and REE-associated phosphatization (n = 1) (Table 1). At Miners Hollow, all modes of preservation observed in this study were represented. Fossils with sclerotized cuticle, e.g., non-biomineralized arthropod carapaces (Appendix A) and feeding appendages (Appendix A, Fig. 3C), *Wiwaxia* spines (KUMIP 490944, Appendix A), *Selkirkia* tubes (Fig. 4D), *Sphenoecium* tubes (Fig. 3A), and *Acinocricus* spines (Fig. 2B), are predominantly preserved as carbonaceous compressions with associated iron minerals. Cellular tissue, e.g., *Eldonia* (Fig. 5 C,D), the everted pharynx of *Utahscolex* (KUMIP 490902; Whitaker et al., 2020) and the eggs of *Waptia* cf. *W. fieldensis* (KUMIP 314032; Moon et al., 2021), exhibit additional modes of preservation, including phosphatization and aluminosilicification (Fig. 5C, D). Preservation quality and diversity is similar in the Cycle 3 and Cycle 6 intervals.

All modes of preservation are also represented at Antimony Canyon. Sclerotized cuticle is preserved through carbonaceous compressions and pyritization, e.g., non-biomineralized arthropod carapaces (KUMIP 491057, Appendix A; KUMIP 135145, Appendix A) and feeding appendages (Fig. 2A), *Wiwaxia* spines (Fig. 2D), *Selkirkia* tubes (Fig. 4E), and *Sphenoecium* tubes (KUMIP 514259, Appendix A). An isolated *Acinocricus* spine, KUMIP 490967 (Appendix A) is preserved by aluminosilicification. The cellular tissue of *Eldonia* (Fig. 5A) is preserved by REE-associated phosphatization. An isolated *Hurdiid* carapace (KUMIP 491057) has a patchy association with Ca (Appendix A).

Cataract Canyon shows more limited preservation pathways, though this may reflect unequal sampling, and thus fewer available samples, within the Wellsville Mountains compared to other localities (Table 1; Whitaker and Kimmig, 2020). Sclerotized *Selkirkia* tubes (Fig. 4A) and *Acinocricus* spines (KUMIP 491082; Appendix A) are preserved mainly through pyritization with restricted areas as carbonaceous compressions. The *Eldonia* specimen (Fig. 5B) from Cataract Canyon shows the REE-associated phosphatization that also occurs in examples from elsewhere.

The sample of soft-bodied preservation from High Creek is limited to two taxa, *Selkirkia* (Fig. 4B) and *Sphenoecium* (Appendix A). Both are preserved through pyritization weathered to iron oxide. The preservation quality is poor, representing only the outline of the specimens.

*Selkirkia* (USNM 768408; Fig. 4F) is the only known genus showing soft-bodied preservation from Blacksmith Fork (based on just six *Selkirkia* specimens at the USNM). It is preserved mainly through pyritization, with very limited carbon outlines (Fig. 4F). The entire exposure of the Langston Formation at Blacksmith Fork is just 9 m, in contrast to other Spence Shale exposures which exceed 100 m at Oneida Narrows and Miners Hollow (Liddell et al., 1997; Kimmig et al., 2019).

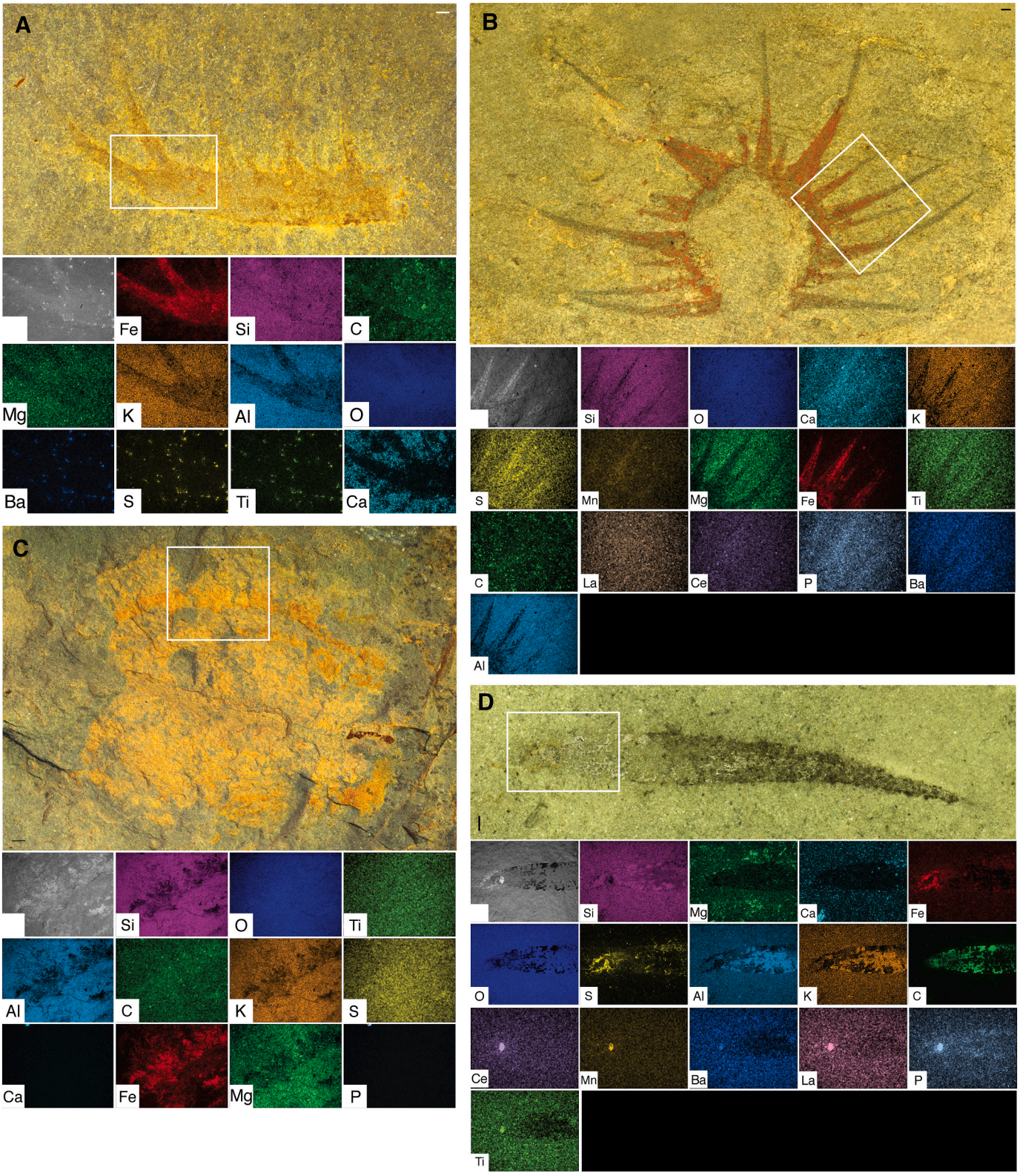


**Fig. 2.** Images and associated SEM–EDS elemental maps of the area highlighted by boxes in the pictures of selected fossils of diverse preservation from the Spence Shale. Elements mapped are noted in lower left corner, initial grey image is backscatter image of mapped area. A) KUMIP 204777, *Sidneyia?*, isolated feeding appendage. B) KUMIP 314131, *Acinocricus*, isolated dorsal spine set. C) KUMIP 558518, *Dioxycaris*, isolated carapace. D) KUMIP 204366, *Wiwaxia*, isolated spine. Scale bars represent A, B, D: 500 μm; C: 1 mm.

Spence Gulch represents a middle ground between the highly diverse preservation pathways of the Wellsville Mountain localities, and the limited preservation of Blacksmith Fork and High Creek (Kimmig et al., 2019). Two bradoriid carapaces were collected in-situ from levels 4 m apart. KUMIP 579391 (Appendix A) is heavily enriched in P, in contrast to KUMIP 579390 (Fig. 3B). The carapace of *Dioxycaris* (Fig. 2C), is not enriched in Ca or P, but is preserved mainly as iron sulfides. It remains uncertain whether these differences represent taxonomic differences in original shell composition, or variation in depositional conditions within this locality.

### 4.1. Kerogenization

Preservation dominated by kerogenization or carbonaceous compression is present in 18 specimens from 4 localities (Miners Hollow, Antimony Canyon, Spence Gulch, and Blacksmith Fork), but is largely limited to small, visibly dark and/or reflective patches. Taxa in which carbon dominates are *Wiwaxia, Eldonia,* Hurdidae, and *Sphenoecium*. The fossils preserved in this manner illustrate fine morphological details. The carbon distribution in the *Wiwaxia* specimens (KUMIP 204366, 490944) clearly shows the striated 'ribbing' of the spines, whereas such features are less distinct in other taphonomic modes such as pyritization (Fig. 2D, Appendix A, respectively). Carbon in the analyzed specimens tends to be

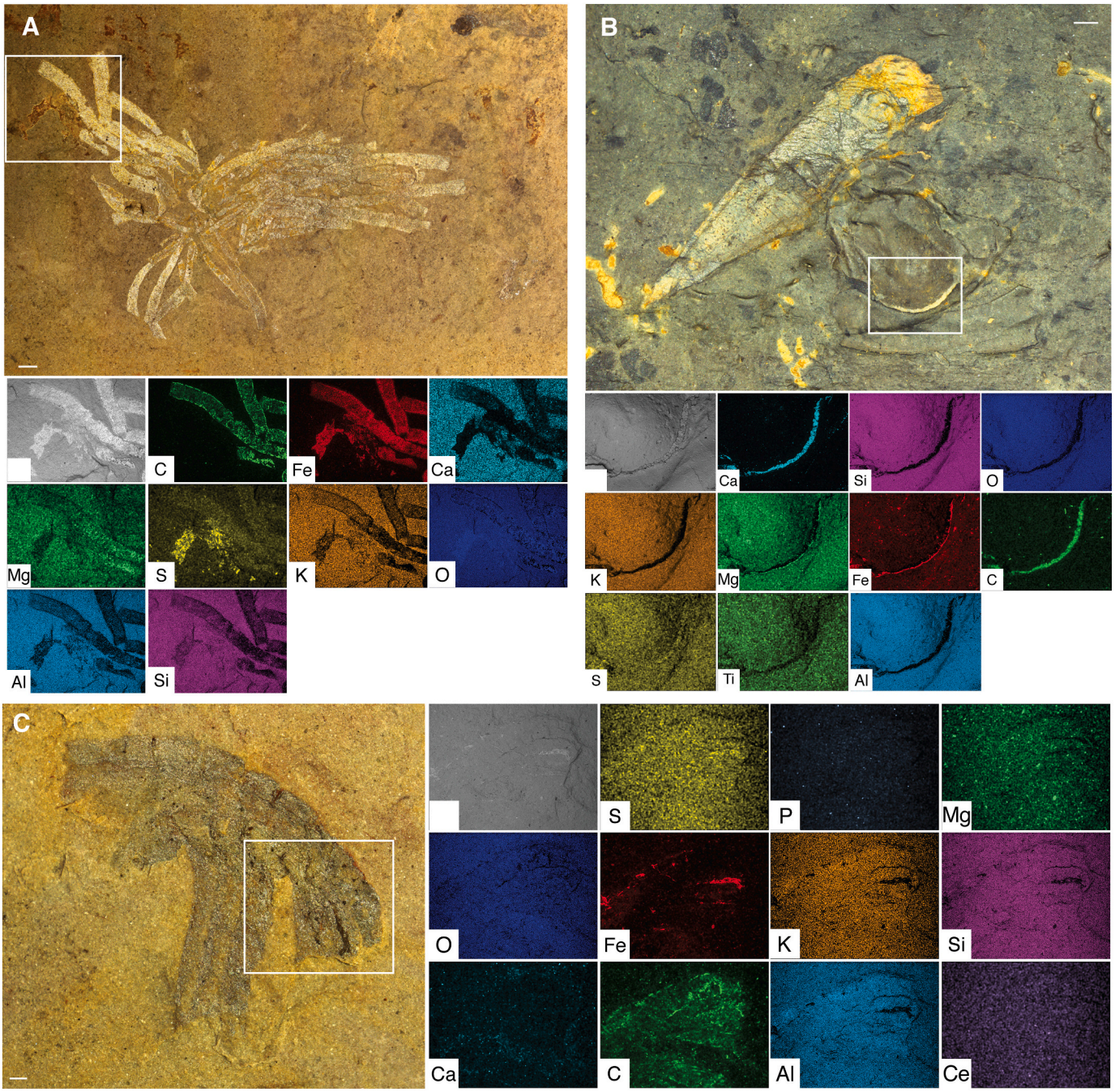


**Fig. 3.** Images and associated SEM–EDS elemental maps of the area highlighted by boxes in the pictures of selected fossils of diverse preservation from the Spence Shale. Elements mapped are noted in lower left corner, initial grey image is backscatter image of mapped area. A) KUMIP 495314, *Sphenoecium wheelerensis.* B) KUMIP 579390, Bradoriid, isolated carapace. C) KUMIP 491056, Hurdiid, isolated feeding appendage. Scale bars represent A, B: 1 mm; C: 500 μm.

concentrated along annulations, edges, and folds, where the overlapping cuticle is thicker. For example, in the hurdiid element (KUMIP 491056), the boundaries of the podomeres are clearly delineated by observable carbon films, which are also evident in the EDS maps (Fig. 3C). Two of the *Sphenoecium* specimens (KUMIP 495314, 514259) from the Wellsville Mountains localities are preserved as highly reflective carbon films, exhibiting parallel striations of the fusellar construction (Fig. 3A, Appendix A, respectively). However, some specimens with comparable dark coloration exhibit low carbon concentrations in elemental maps.

### 4.2. Pyritization

Pyrite or its iron oxide- and/or oxyhydroxide-weathering products are present in 35 analyzed samples representing all six sampled localities. While oxidized pyrite preservation is evidenced by a rusty red-orange coloration of the fossils, this mode of preservation is confirmed here by the presence of iron-bearing framboidal textures indicating weathering-induced pseudomorphs after original pyrite. Iron-bearing mineral concentrations usually follow the margins of the specimens.

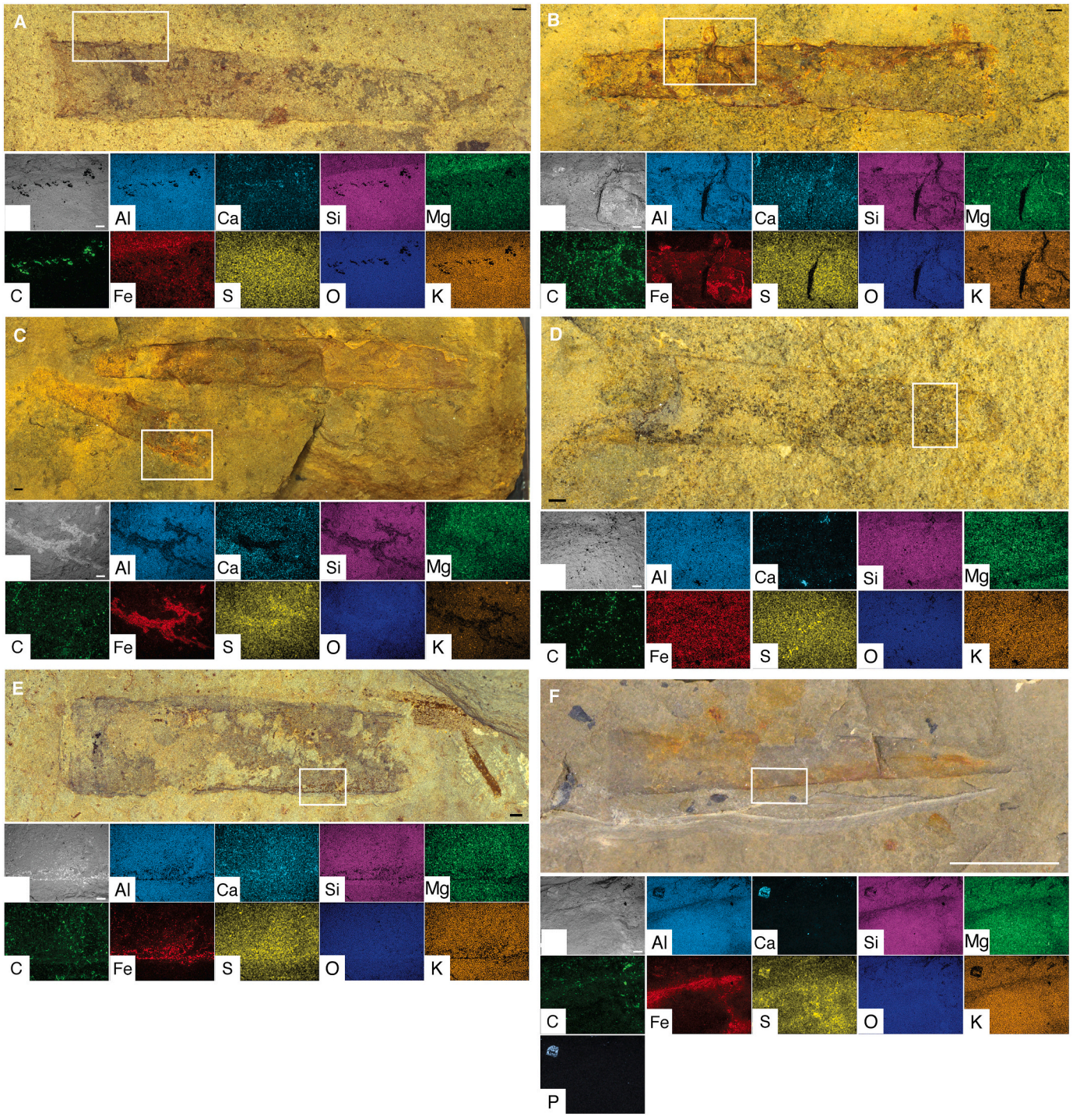


**Fig. 4.** *Selkirkia* specimens from the Spence Shale with associated SEM–EDS elemental maps of the area highlighted by boxes in the pictures. Elements mapped are noted in lower left corner, initial grey image is backscatter image of mapped area. A) KUMIP 563151, Cataract Canyon. B) KUMIP 563145, High Creek. C) KUMIP 563150, Spence Gulch. D) KUMIP 314158, Miners Hollow. E) KUMIP 144845, Antimony Canyon. F) USNM 768408, Blacksmith Fork. Scale bars represent A-E: 1 mm; F: 1 cm.

KUMIP 563145, *Selkirkia*, typifies this preservation style, with large patches of orange iron staining concentrated around the edges of the tube (Fig. 4B, Appendix A). The presence of unweathered pyrite is intermittent and varies within specimens. In KUMIP 135145, *Dioxycaris*, the carapace preserves scattered pyrite euhedra on the upper edge and more densely packed pyrite framboids on the lower edge, as evidenced by coincident concentrations of Fe and S (Appendix A). Elevated concentrations of barium are found alongside iron preservation in some specimens, such as KUMIP 135145 (Appendix A) and KUMIP 144845 (Appendix A). The apparent presence of Ti is likely an instrumental artifact, owing to the overlap of the barium Lα and titanium Kα x-ray energies and the direct spatial overlap in their elemental maps (e.g., KUMIP 135145).

### 4.3. Phosphatization

The presence of calcium and phosphorus, which together reflect taphonomic phosphatization, is found sporadically in nine specimens from Antimony Canyon, Cataract Canyon, Miners Hollow, and Spence Gulch. Two bradoriid specimens from Spence Gulch, KUMIP 579390, 579391 (Fig. 3B, Appendix A respectively), show elevated calcium in their carapace, but elevated phosphorus is also evident in KUMIP 579391. Some plates of a specimen of *Utahscolex ratcliffei* from Miners Hollow, counterpart KUMIP 204390 and part UMNH IP 4696, are enriched in Ca, although they are mainly preserved in iron oxides (Fig. 2d, Whitaker et al., 2020). Plates in a second Miners Hollow specimen of *U. ratcliffei,* KUMIP 490902, show elevated Ca and P and in some cases Mg (Fig. 3g, Whitaker et al., 2020). In four eldoniid specimens from Miners Hollow (KUMIP 510274 and KUMIP 510275), Cataract Canyon (KUMIP 490937), and Antimony Canyon (KUMIP 204370), specific anatomical tissues are intermittently preserved with localized Ca. A hurdiid feeding appendage from Miners Hollow, KUMIP 491056, has a low elevation of Ca (Fig. 3C). Eggs of a specimen of *Waptia* cf. *W. fieldensis,* KUMIP 314032, are phosphatized, shown in this case to be controlled by whether or not the egg envelope ruptured resulting in an open or closed environment (Moon et al., 2021).

### 4.4. Aluminosilicification

Aluminosilicification, or preservation via clay mineral templating, is observed in seven specimens from three localities (Miners Hollow, Cataract Canyon, and Spence Gulch). These seven specimens represent the genera *Sidneyia*? (KUMIP 204779, Table 1), *Acinocricus* (KUMIP 490967, Table 1*)*, *Selkirkia* (KUMIP 563151, Table 1), *Utahscolex* (KUMIP 490902, Whitaker et al., 2020), unidentified vermiform organisms (KUMIP 314111, Broce and Schiffbauer, 2017; KUMIP 557975, Table 1), and an indeterminate organism (KUMIP 314186, Broce and Schiffbauer, 2017). Compositionally, these specimens show slightly elevated concentrations of Si and Al compared to the matrix.

### 4.5. Rare earth concentrations associated with Eldonia

All four analyzed specimens of *Eldonia ludwigi*, representing three separate localities (Antimony Canyon, Cataract Canyon, and Miners Hollow), revealed a unique preservation mode (Fig. 5A–D). In specimen KUMIP 204370, the coiled sac is preserved by both reflective patches and darker patches (Fig. 5A, Appendix A). The reflective patches contain high concentrations of C associated with Ba, Mn, P, and rare earth elements (REE) Ce and La, whereas the darker patches show only elevated Ca. The patchy distribution of P enrichment in KUMIP 204370 (Fig. 5A) (i.e., it only occurs in the 'reflective' areas) could be due to the differentiation of outer and inner tissue layers in the gut tract of *Eldonia* as observed by Butterfield (1996). Thus, the P enrichment in this specimen may indicate that the inner layer of the gut tract presents a micro environment favoring phosphate precipitation. The bifurcating internal lobes in KUMIP 204370 are preserved as darker, non-reflective areas but are not clearly differentiated from the matrix. In KUMIP 510274 and 510275 (Fig. 5C–D), the coiled sac is preserved as a darkened area with elevated C, and a more reflective area with concentrations of Fe and Mg. Scattered throughout are bladed phosphatic crystals containing Ce and La. The fourth specimen, KUMIP 490937 (Fig. 5B), preserves concentrated detritus, collected along the margins of the poorly preserved *Eldonia*. Scattered crystals within the specimen are enriched with La, Ce, Ba, Mn, P, and irregularly, S. The margin shows elevated C, Fe, and Mg.

### 4.6. Histology summary

In terms of fossilized tissues, a majority of the eumetazoan genera 73% ($n = 50$) preserve one tissue type, 20% ($n = 14$) preserve two tissue types, and 7% (n = 5) preserve three types (Appendix B). The most common tissue type is a biomineralized skeleton (68% of genera), followed by sclerotized tissue (26%), cuticular tissue (19%), soft internal cellular tissue (13%), and soft external cellular tissue (7%). In genera with two tissues present, the two most common tissue types to occur together are sclerotized and cuticular tissue ($n = 7$), followed by sclerotized tissue and soft internal cellular tissue ($n = 2$), and biomineralized skeleton and soft internal cellular tissue (n = 2). Of genera preserving three tissue types, the most common co-occurrence is a biomineralized skeleton, cuticular tissue, and soft internal cellular tissue ($n = 3$).

## 5. Discussion

### 5.1. Variation in preservation by locality

The sampled genera show intra- and inter-locality variation in preservation. Each locality displayed multiple modes of preservation, including variation between and within stratigraphic horizons.

The influence of locality on preservation is largely limited to the impact of weathering. This is typified by the Spence Gulch locality, which is heavily wooded and located close to Mill Creek. Specimens recovered from float at this locality are predominantly preserved as iron oxides. Specimens recovered in situ (e.g., Fig. 2C; KUMIP 558518, Appendix A) show localized iron sulfide preservation particularly at the base of the exposure where the rocks appear less weathered. The majority of Spence Shale exposures are located on the slopes of steep gullies formed by extensive erosion, and others (i.e., Oneida Narrows) are located on the banks of small rivers. Such settings favor weathering of pyrite to iron oxides.

Soft-bodied preservation declines in abundance from localities in the Wellsville Mountains to those in the Wasatch Range and Spence Gulch in the Bear River Range. Miners Hollow is the most distal of the Wellsville Mountain localities (Kimmig et al., 2019). Geochemical analyses of sediment samples from Spence Gulch, Oneida Narrows, Miners Hollow, and High Creek indicate a predominantly oxic depositional environment, with low bioturbation (Kloss et al., 2015). Therefore, the variability in modes of preservation is likely linked to other second-order environmental factors ("distal factors" of Cai et al., 2012), such as sealing of the sediment-water interface, diagenetic fluid flow, and modern weathering.

Spence Shale specimens were buried rapidly, showing a high fidelity of preservation of labile tissues, although some show initial signs of degradation (e.g., uneven *Utahscolex* tissue margins; Fig. 3a, Whitaker et al., 2020). Collapse preceded preservation, with few exceptions (e.g., *Waptia* cf. *W. fieldensis* eggs), suggesting that this was likely due to decay. This is also supported by the incomplete nature of a large proportion of the Spence Shale soft-bodied fossils (Whitaker and Kimmig, 2020). Early diagenetic processes include phosphatization and pyritization of soft tissues (e.g., bradoriid carapaces, *Waptia* cf. *W. fieldensis* eggs). During multiple orogenic events, the Spence Shale underwent metamorphic alteration, kerogenizing organic carbon, and altering minerals (e.g., apatite to monazite; Broce and Schiffbauer, 2017). Magnesium-rich fluid movement through the Spence Shale dolomitized

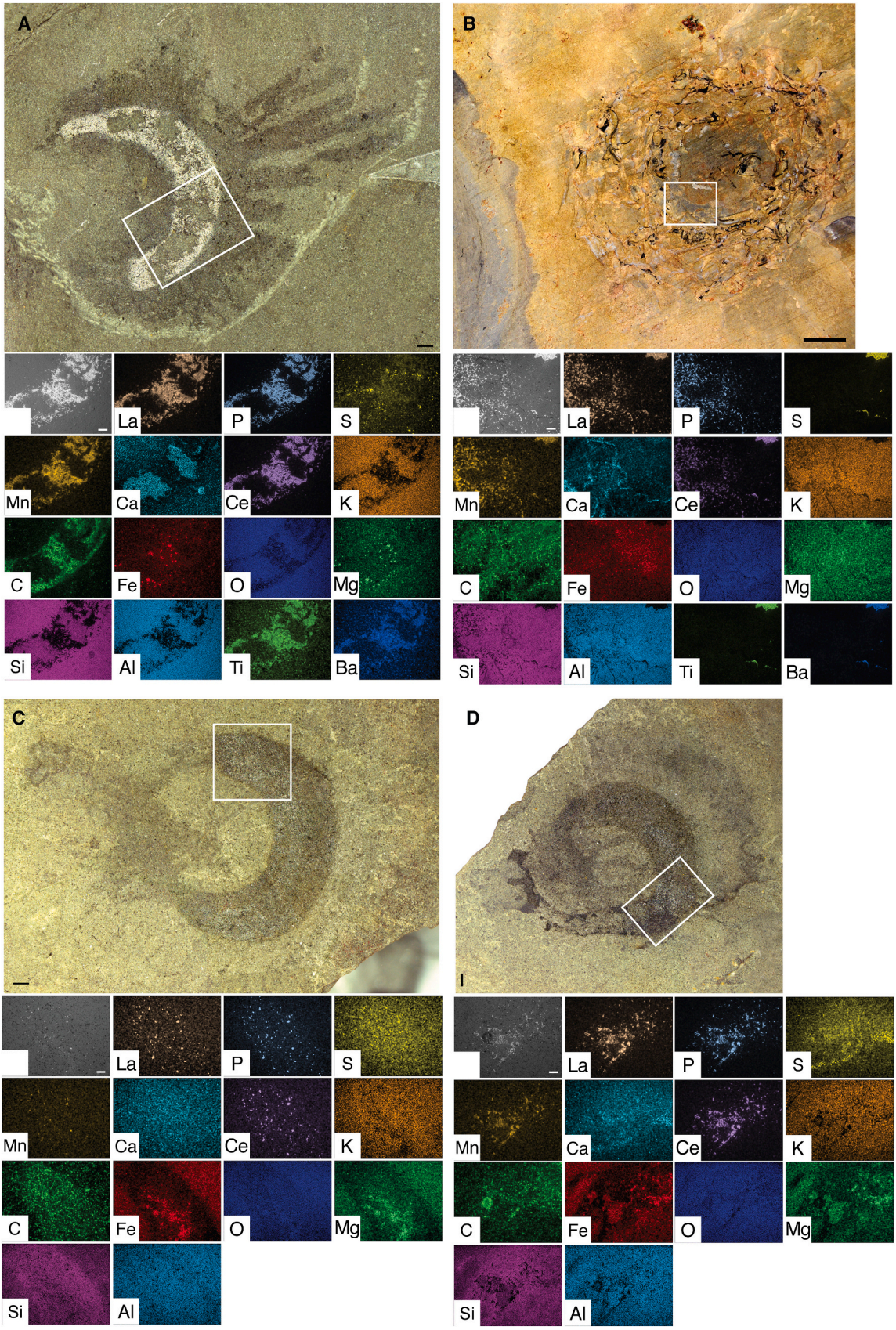


**Fig. 5.** *Eldonia ludwigi* specimens from the Spence Shale with associated SEM–EDS elemental maps of the area highlighted by boxes in the pictures. Elements mapped are noted in lower left corner, initial grey image is backscatter image of mapped area. A) KUMIP 204370, Antimony Canyon. B) KUMIP 490937, Cataract Canyon. C) KUMIP 510275, Miners Hollow. D) KUMIP 510274, Miners Hollow. Scale bars represent A, C, D: 1 mm; B: 1 cm.

calcium-rich features (e.g., the plates of *Utahscolex*). Pyrite was altered during diagenesis and weathering, forming iron oxides and barite (e.g., KUMIP 135145, Appendix 1; KUMIP 314191, KUMIP 314215; Broce and Schiffbauer, 2017).

### 5.2. Variation in preservation by taxa

The priapulid *Selkirkia* is the only genus found at all six sampled localities (Fig. 4A–F). The isolated tubes are reddish-orange, and predominantly preserved as pyrite and iron oxides, with patchy carbonaceous areas. The margins of the tubes show the strongest signal, and the annulations on the tubes are rarely evident (Fig. 4E). None of our analyzed specimens preserve the body, and possible soft parts are known in only one specimen, KUMIP 314115 (Kimmig et al., 2019, fig. 5d). The poor preservation of *Selkirkia* in the Spence Shale contrasts with that in other Cambrian BST Lagerstätten, such as the Xiaoshiba and Chengjiang, where the pharynx, digestive tract, and gut contents are preserved (Tian et al., 2015; Wang et al., 2021; Yang et al., 2021b). A higher proportion of specimens of *Selkirkia* from the Burgess Shale and Wheeler Lagerstätten also preserve soft parts, approximately 20% and 33%, respectively (Conway Morris and Robison, 1986). The tube of *Selkirkia* tube is more decay resistant than its trunk, but other stem-priapulid body fossils from Miners Hollow preserve soft tissues such as the everted proboscis and gut tract (Whitaker et al., 2020). In the Chengjiang Lagerstätte, *Selkirka* tubes, body fossils, and eggs in the tubes are preserved in carbon and iron oxides, formed by weathering of pyrite microcrystals (Wang et al., 2021; Yang et al., 2021b). The similarities in the mode of *Selkirkia* preservation between the Spence Shale and the Chengjiang Lagerstätte emphasizes differences in the quality of preservation – it is likely some of the "empty" tubes represent exuviae of the molting *Selkirkia*, but does not fully explain the lack of soft parts.

*Acinocricus* was sampled from three localities in the Wellsville Mountains (Miners Hollow, Cataract Canyon and Antimony Canyon), where it is represented by the cuticle of isolated body segments (Fig. 2B, Appendix A). They are preserved in multiple ways: pyritization (Fig. 2B; KUMIP 4911082, Appendix A), aluminosilification (KUMIP 490967, Appendix A), and phosphatization (Fig. 2B). Disarticulated spines are most common, but articulated fossils of *Acinocricus* are known from the Wellsville Mountains (Caron and Aria, 2020). In KUMIP 314131 (Fig. 2B), the enrichment of Fe and S echoes the "cone-in-cone" spine structure reported by Caron and Aria (2020).

The two isolated spines of *Wiwaxia,* KUMIP 204366 (Fig. 2D) and KUMIP 490944 (Appendix A), are predominantly preserved as carbon films, as well as Fe enrichment. Acicular crystals of iron sulfide were reported within the striations on *Wiwaxia* spines from the Burgess Shale (Smith, 2014), which are predominantly carbonaceous (Butterfield et al., 2007). In the Spence Shale specimens, the striation boundaries are preserved as cracks or terminations of the carbon film (Fig. 2D) or as concentrations of carbon (Appendix A).

Two bradoriid carapaces (KUMIP 579390, Fig. 3B; and KUMIP 579391, Appendix A) are among the few Spence Shale specimens primarily preserved as calcium carbonate or calcium phosphate. This is interpreted as diagenetic and not useful as a taxonomic indicator (Vannier et al., 2005; Streng et al., 2008). The preservation of the Spence Shale bradoriids is similar to those found elsewhere (e.g., Streng et al., 2008; Peel et al., 2021), but differs from other Spence Shale soft-bodied arthropods which do not show the same diagenetic calcium enrichment (e.g., *Dioxycaris*), although the sample size is limited.

Phosphatic material, presumably apatite, is present in the eggs of a specimen of *Waptia* cf. *W. fieldensis* (KUMIP 314032) (Moon et al., 2021). The preservation of these eggs in the Spence Shale (preservation through phosphatization and carbonaceous compressions and some differentiation of the inner and outer layers of the eggs) is similar, but less detailed, to that of *W. fieldensis* eggs from the Burgess Shale, where an inner portion is preserved in carbon, calcium, phosphorus, iron, and sulfur, and an outer portion in aluminum and potassium (Caron and Vannier, 2016). This differs in detail to the eggs of *Chuandianella ovate*, a bivalved waptiid arthropod from the Chengjiang Lagerstätte. Its eggs are primarily preserved in iron oxides, the weathering product of authigenic pyrite, with additional slight enrichment in phosphorus, sulfur, carbon, cobalt, platinum, and copper (Ou et al., 2020).

Preservation differences within taxa are largely limited to differences in specific tissue type, i.e., gut tract phosphatization or pyritization. Gut tract phosphatization is found in the Wellsville Mountain eldoniid specimens (discussed below), and an *Anomalocaris* specimen from Miners Hollow, KUMIP 314037 (Appendix A). The phosphatized patches of *Anomalocaris* are located medially on the specimen, where the digestive system would have been located (Briggs et al., 2008). Densely packed parallel fibers are arranged across the patches, potentially representing adjacent muscle fibers or mid-gut glands (Vannier et al., 2014).

#### 5.2.1. REE enrichment

The *Eldonia* specimens are all enriched in the light Rare Earth Elements (LREE) La and Ce, in contrast to other currently sampled taxa in the Spence Shale. The LREE are associated with P, Ba, Ti, and Mn, suggesting that apatite has been altered to monazite, a LREE-bearing phosphatic mineral. Monazite has been identified associated with the gut tracts of two vermiform specimens from the Spence Shale (Broce and Schiffbauer, 2017), in isolated areas on the carapace of *Canadaspis* and surrounding sediment from the Pioche Shale Lagerstätte (Moore and Lieberman, 2009), and in association with numerous fossils from the Sirius Passet Lagerstätte (Nielsen et al., 2021). In the Pioche Shale, the monazite is found in both the fossil and sediment. Moore and Lieberman (2009) interpreted it as diagenetic rather than detrital in the sediment. REE (including La and Ce) in phosphatized palaeoscolecid casts from the Ordovician Tafilalt Konservat-Lagerstätte, were likewise interpreted as diagenetic (Gutiérrez-Marco and García-Bellido, 2015). In the Sirius Passet Lagerstätte, monazite was most commonly found in the adjacent sediment, and at the tissue-sediment interface, rather than directly associated with phosphatized or previously phosphatized tissues (Nielsen et al., 2021). The alteration of phosphate to monazite is interpreted as the result of metamorphic alteration of original phosphatic preservation (Nielsen et al., 2021).

Monazite is formed from the dissolution of LREE-bearing apatite, potentially identifying apatite, or an apatite precursor, as the authigenic mineral preserving the gut tracts of the eldoniids, as suggested for the vermiform organisms in the Spence Shale (Broce and Schiffbauer, 2017). The presence of monazite in *Eldonia* specimens is independent of locality, and appears to be taxon-specific, as co-occurring species (Table 1) did not show similar concentrations of REE with the exception of a well-defined patch of REE-enriched phosphate at the base of a *Wiwaxia* spine (KUMIP 204366; Fig. 2D). KUMIP 490937 (Fig. 5B) from Cataract Canyon preserves aggregated detritus around a poorly-preserved eldoniid disk suggesting a high-energy environment where biomineralized fragments were swept by currents and collected around the eldoniid on the sediment surface, as was observed in examples from the Miaotianshan Shale (Vannier and Chen, 2005). Despite the degradation of this eldoniid, it shows REE enrichment. Previously analyzed Spence Shale specimens where monazite is associated with a gut tract (Table 1; Broce and Schiffbauer, 2017) cannot be identified to taxon, although a plausible interpretation could be the degraded gut of an eldoniid.

Phosphatization associated with gut tract preservation has been reported in numerous taxa from other BST Lagerstätten, including trilobites (Weeks Formation), radiodonts (Spence Shale and Burgess Shale), *Leanchoilia, Odaraia, Opabinia, Alalcomenaeus, Perspicaris, Naraoia, Burgessia, Plenocaris, Molaria, Sidneyia, Isoxys* (Burgess Shale), *Pambdelurion* and *Campanamuta* (Sirius Passet Lagerstätte) and an indet. *Fuxianhuia*-like arthropod (Kaili Formation) (Briggs and Whittington, 1985; Briggs and Collins, 1999; Butterfield, 2002; Zhu et al., 2004; Lerosey-Aubril et al., 2012; Schiffbauer et al., 2014; Vannier et al., 2014; Strang et al., 2016; Zacaï et al., 2016). The preservation of digestive

systems is likely facilitated by an internal source of phosphate in combination with a closed-system post-mortem (Butterfield, 2002; Lerosey-Aubril et al., 2012; Strang et al., 2016). Possible ingested sources of P have been suggested to include microbial mats (Lerosey-Aubril et al., 2012) and other arthropods (Strang et al., 2016); although "spherites" rich in Ca and P, a common mineral storage feature in the midgut tissue in modern chelicerates, crustaceans, and insects, also provide a source of P (Butterfield, 2002; Lerosey-Aubril et al., 2012; Zacaï et al., 2016).

Modern non-predatory benthic vertebrates and invertebrates have higher concentrations of REE than their predatory counterparts (Mayfield and Fairbrother, 2015; Amyot et al., 2017). Macro-invertebrates that feed by ingesting organic particulates from the sediment are positively correlated with REE concentrations, more so than other feeding styles, indicating that sediment ingestion is an effective bioaccumulation pathway (Pastorino et al., 2019). Marine invertebrates (e.g., scallops, amphipods) accumulate REE despite their relatively low concentrations in seawater, also indicating that the source is ingested via sediment (Bustamante and Miramand, 2005; Palmer et al., 2006). *Eldonia* has been interpreted as a nektobenthic filter feeder (Caron et al., 2010; MacGabhann, 2012), and the concentration of REE in its gut, as preserved, may be consistent with an in-vivo accumulation, that might have led to elevated levels of REE in the carcass, which were then preferentially incorporated in the monazite.

An alternative explanation, and more consistent with previous interpretations of REE accumulation, is that phosphate in the coiled sac of *Eldonia* favored the accumulation of LREE during diagenesis. Phosphate and calcium are stored in the gut of many arthropods (e.g., Zacaï et al., 2016). REE (Y, Nd) and Sr are enriched in the phosphatized soft tissue of decapod shrimp from the Upper Cretaceous Djebel Oum Tkout Lagerstätte (Gueriau et al., 2014). The REE element Y is concentrated in the phosphatized gut tract of penaeoid shrimp from the Triassic Paris Biota (Brayard et al., 2019). A comparison of modern and Miocene gastropods, echinoderms, and bivalves concluded that significant concentrations of REE elements are a diagenetic signal (MacFadden et al., 2015).

The "open system" behavior of apatite is well known, providing readily available sites for elemental replacement within the lattice (Kocsis et al., 2010; Herwartz et al., 2011; Herwartz et al., 2013; Keenan, 2016; Zhang et al., 2016; Decrée et al., 2018; Kocsis et al., 2020). Trace element uptake and exchange fluctuate throughout early and late diagenesis, reflecting changes in the composition of the fluid source (Herwartz et al., 2011: Herwartz et al., 2013; Decrée et al., 2018). Monazite has been experimentally formed from metasomatic dissolution of LREE-apatite under a range of simulated metamorphic temperatures and pressures, including greenschist conditions (Harlov and Förster, 2003). In this scenario, the coiled sac was diagenetically enriched in REE following initial phosphatization. The REE-enriched apatite was then altered to monazite during later diagenesis.

Several other wholly or partially phosphatized specimens do not show the same REE enrichment, but this may reflect limited sampling. Two bradoriid carapaces (KUMIP 579390 and KUMIP 579391, Fig. 3B, Appendix A, respectively) show diagenetic phosphate and calcium enrichment of the original unmineralized shell, but lack REE enrichment. Diagenetic phosphatization has been observed in other bradoriids (e.g., Peel et al., 2021) and might suggest oscillating pore-water redox during periods of prolonged oxygen depletion in the Spence Shale, which would favor phosphate nucleation during early diagenesis (Pruss et al., 2018). The eggs of *Waptia* cf. *W. fieldensis* (KUMIP 314032; Moon et al., 2021) and phosphatic patches, which might represent digestive glands (Vannier et al., 2014), in *Anomalocaris* KUMIP 314037 (Appendix A), have not been analyzed for REE. The problematic shell-bearing *Armilimax* (KUMIP 490943) and the palaeoscolecid *Utahscolex* (KUMIP 204390/ UMNH IP 4696 and KUMIP 490902), which preserve gut tracts, show diagenetic alteration, i.e., the dolomitization of the original calcium carbonate shell and phosphatic plates, respectively, but lack REE enrichment within the gut tract (Whitaker et al., 2020; Kimmig and Selden, 2021).

Based on the current data from this and previous studies, it is impossible to determine whether the REE enrichment in the *Eldonia* specimens represents a biological or strictly diagenetic signal. Further analyses of *Eldonia* and additional phosphatized specimens from the Spence Shale and other deposits will elucidate whether this pattern is constrained to this genus, and determine whether the REE enrichment is limited to phosphatized gut tracts or additional tissues.

### 5.3. Comparison to other BST deposits

The Spence Shale is one of five Cambrian Lagerstätten in Utah, the others located in the House Range (the 'deep' Wheeler, Marjum and Weeks formations), and the Drum Mountains (the 'shallow' Wheeler Formation). In the Wheeler Formation, the extensive preservation of carbonaceous compressions has been interpreted as the result of carbonate-precipitated occluded porosity in anoxic bottom waters owing to the precipitation of carbonate bed seals (Gaines et al., 2005). Some Wheeler Formation soft-bodied arthropods are preserved through pyritization, a product of anaerobic sulfate reduction (e.g., Lerosey-Aubril et al., 2020). Articulated palaeoscolecid plates from the Marjum Formation are preserved through Fe, Mg, Ca, and P, but carbonaceous remains of tissues are absent (Leibach et al., 2021). This differs from the preservation of palaeoscolecids from the Spence Shale, which preserve labile tissues of the proboscis and gut tract in addition to the plates (Whitaker et al., 2020).

The representation of multiple modes of preservation, even within specimens, is shared with other BST deposits. The Chengjiang Biota features phosphatization, pyritization, Fe-rich aluminosilicates, and organic films (Zhu et al., 2005). Non-mineralizing organisms of the Chengjiang biota are predominantly preserved through Fe-oxides, whereas phosphatization is rare (Gabbott et al., 2004; Zhu et al., 2005). The Spence Shale, like the Chengjiang Biota, has undergone weathering, altering pyrite to Fe-oxides (Zhu et al., 2005). Compared to the Burgess Shale, the Spence Shale represents a different depositional environment: more rapid fluctuations between oxic, dysoxic, and anoxic conditions, limited to no transport, and less potential for immediate burial (Garson et al., 2012; Kloss et al., 2015). The Burgess Shale also features phosphatization and pyritization in addition to the predominant preservation through carbonaceous compressions (García-Bellido and Collins, 2006; Gaines et al., 2008; Gaines et al., 2012; Gaines, 2014; Vannier et al., 2014; Zacaï et al., 2016). Phosphatization is overwhelmingly found associated with gut tract preservation. Pyritization is rare in the Burgess Shale: a sample of more than 1000 analyzed *Marrella* specimens included only two with areas of pyritization (García-Bellido and Collins, 2006). Pyrite is also rarely associated with gut tract preservation (Butterfield, 2002; Lin and Briggs, 2010). Both the Spence Shale and the Burgess Shale have undergone metamorphism: the Burgess Shale has undergone multiple stages of greenschist and subgreenschist metamorphism, with variable impact on preservation based on position relative to the escarpment (Powell, 2003). The metamorphism of the Burgess Shale primarily affects kerogenization and late-stage aluminosilification, whereas metamorphism of the Spence Shale also affected modes of mineralization (e.g., phosphatization and dolomitization).

In addition to the familiar preservation modes of BST deposits, association of unusual minerals with soft-tissues occurs in the Burgess Shale (Pushie et al., 2014), where possible biogenic copper, in the form of chalcopyrite, was reported in the arthropod *Marrella*, although the evidence for a biogenic origin of chalcopyrite has since been disputed (Gaines et al., 2019). Microbially mediated silver has been reported from the Ravens Throat River Lagerstätte (Kimmig and Pratt, 2022), indicating that biogenic minerals might be more common in BST deposits than previously thought.

Using the taphonomic comparison metrics of Saleh et al. (2020a), the Spence Shale shares most characteristics with the Fezouata Biota out of the three Lagerstätten considered (Fezouata, Burgess Shale and

Chengjiang). A majority of specimens preserve only one of the tissue types in contrast to the Burgess Shale or the Chengjiang, where multiple tissue types are more common in a fossil. The average number of tissue types per genus is comparable to that in the Fezouata Biota (1.333 in the Spence Shale, 1.316 in the Fezouata) (Appendix B). Soft cellular tissue, either external or internal, is rarely preserved in the absence of more decay-resistant biomineralized, sclerotized, or cuticular tissue, where they co-occur. The Spence Shale, like the Fezouata, has undergone modern weathering, affecting the original carbonaceous compression and pyrite preservation (Saleh et al., 2020b, 2021). The carbonate cement 'caps', interpreted as sealing the sediment surface and promoting preservation in other Lagerstätten (Gaines et al., 2012; Saleh et al., 2020b), are absent in the Spence Shale, as at Fezouata, creating conditions favoring pyritization.

## 6. Conclusion

Based on this study and previous work, the primary processes influencing preservation in the Spence Shale are, sequentially, survival of organic remains, early taphonomic precipitation of phosphate and pyrite, maturation of carbonaceous remains to kerogen, later metamorphic alteration of phosphate to monazite, and other effects of modern weathering (e.g., oxidation of pyrite). These preservation modes are comparable to preservation types from other BST deposits, against the backdrop of an atypical dynamic redox environment across the Spence depositional settings. Diagenesis has resulted in alteration of the REE-enriched phosphate in the gut tracts of *Eldonia.* The apparently unique association of REE elements with *Eldonia* in the Spence Shale warrants further investigation, as REE enrichment in BST preservation is rare. A likely contributing factor is the exclusion of REE and trace elements in previous analyses. Further SEM-EDS analyses of eldoniids from the Spence Shale and other BST Lagerstätten, as well as detailed studies of their anatomy and gut contents, will elucidate whether this pattern reflects their mode of life, or a taphonomic pathway shared by specific tissues in the Spence Shale.

Despite taphonomic conditions that limited preservation in the Spence Shale (e.g., initial decomposition, bioturbation, diagenetic alteration, modern weathering, etc.), exceptional preservation still occurred in a variety of shelf environments. The presence of preserved muscle tissue, eyes, eggs, and the discovery of new taxa emphasize the importance of this Lagerstätte. With continued study, the Spence Shale is "catching up" in importance with better known BST-deposits.

## Declaration of Competing Interest

The authors declare that they have no known competing financial interests or personal relationships that could have appeared to influence the work reported in this paper.

## Acknowledgements

We thank the Gunther family, P. Jamison, and P. Reese for collecting and donating specimens. The authors gratefully acknowledge the contribution of the reviewer J. Vannier, whose comments resulted in improvements and clarifications to the manuscript. This work was supported by an Association of Earth Science Clubs of Greater Kansas City Research Grant, a University of Kansas Biodiversity Institute Panorama Grant, a Geological Society of America Graduate Student Research Grant, and a Paleontological Society Kenneth E. and Annie Caster Student Research Award to AW. JK's work in the Spence Shale has been supported by a Paleontological Society Arthur James Boucot Grant, an Association of Earth Science Clubs of Greater Kansas City Research Grant and a Western Interior Paleontological Society Karl Hirsch Memorial Grant. JK thanks the USDA Forest Service for permits. JDS is supported by NSF CAREER 1652351, and the University of Missouri X-ray Microanalysis Core by NSF IF 1636643.

## Appendix A. Supplementary data

Supplementary data to this article can be found online at https://doi.org/10.1016/j.palaeo.2022.110909.

## References

Amyot, M., Clayden, M.G., MacMillan, G.A., Perron, T., Arscott-Gauvin, A., 2017. Fate and trophic transfer of rare earth elements in temperate lake food webs. Environ. Sci. Technol. 51, 6009–6017. https://doi.org/10.1021/acs.est.7b00739.

Black, B.D., Giraud, R.E., Mayes, B.H., 2000. Paleoseismic Investigation of the Clarkston, Junction Hills, and Wellsville Faults, West Cache Fault Zone, Cache County, Utah. In: Lund, W.R. (Ed.), Paleoseismology of Utah, Utah Geological Survey Special Study 98, vol. 9. Utah Geological Survey, Salt Lake City, pp. 1–23.

Brayard, A., Guériau, P., Thoury, M., Escarguel, G., 2019. Glow in the dark: use of synchrotron μXRF trace elemental mapping and multispectral macro-imaging on fossils from the Paris Biota (Bear Lake County, Idaho, USA). Geobios 54, 71–79. https://doi.org/10.1016/j.geobios.2019.04.008.

Briggs, D.E.G., Collins, D., 1999. The arthropod *Alalcomenaeus cambricus* Simonetta, from the Middle Cambrian Burgess Shale of British Columbia. Palaeontology 42, 953–977. https://doi.org/10.1111/1475-4983.00104.

Briggs, D.E.G., Whittington, H.B., 1985. Modes of life of arthropods from the Burgess Shale, British Columbia. Earth and Environ. Sci. Trans. Royal Soc. Edinburgh 76, 149–160. https://doi.org/10.1017/S0263593300010415.

Briggs, D.E.G., Lieberman, B.S., Hendricks, J.R., Halgedahl, S.L., Jarrard, R.D., 2008. Middle Cambrian arthropods from Utah. J. Paleontol. 82, 238–254. https://doi.org/10.1666/06-086.1.

Broce, J.S., Schiffbauer, J.D., 2017. Taphonomic analysis of Cambrian vermiform fossils of Utah and Nevada, and implications for the chemistry of Burgess Shale-Type preservation. Palaios 32, 600–619. https://doi.org/10.2110/palo.2017.011.

Bustamante, P., Miramand, P., 2005. Subcellular and body distributions of 17 trace elements in the variegated scallop *Chlamys varia* from the French coast of the Bay of Biscay. Sci. Total Environ. 337, 59–73. https://doi.org/10.1016/j.scitotenv.2004.07.004.

Butterbaugh, G.J., 1982. Petrology of the Lower Middle Cambrian Langston Formation, North-Central Utah and Southeastern Idaho (Master's Dissertation). Utah State University, Logan, p. 166.

Butterfield, N.J., 1996. Fossil preservation in the Burgess Shale: reply. Lethaia 29, 109–112. https://doi.org/10.1111/j.1502-3931.1996.tb01845.x.

Butterfield, N.J., 2002. *Leanchoilia* guts and the interpretation of three-dimensional structures in Burgess Shale-type fossils. Paleobiology 28, 155–171. https://doi.org/10.1666/0094-8373(2002)028<0155:LGATIO>2.0.CO;2.

Butterfield, N.J., Balthasar, U.W.E., Wilson, L.A., 2007. Fossil diagenesis in the Burgess Shale. Palaeontology 50, 537–543. https://doi.org/10.1111/j.1475-4983.2007.00656.x.

Cai, Y., Schiffbauer, J.D., Hua, H., Xiao, S., 2012. Preservational modes in the Ediacaran Gaojiashan Lagerstätte: Pyritization, aluminosilicification, and carbonaceous compression. Palaeogeogr. Palaeoclimatol. Palaeoecol. 326, 109–117.

Caron, J.B., Aria, C., 2020. The Collins' monster, a spinous suspension–feeding lobopodian from the Cambrian Burgess Shale of British Columbia. Palaeontology 63, 979–994. https://doi.org/10.1111/pala.12499.

Caron, J.B., Vannier, J., 2016. *Waptia* and the diversification of brood care in early arthropods. Curr. Biol. 26, 69–74. https://doi.org/10.1016/j.cub.2015.11.006.

Caron, J.B., Morris, S.C., Shu, D., 2010. Tentaculate fossils from the Cambrian of Canada (British Columbia) and China (Yunnan) interpreted as primitive deuterostomes. PLoS One 5, 1–13. https://doi.org/10.1371/journal.pone.0009586.

Chen, C.Y., Maloof, A.C., 2017. Revisiting the deformed high shoreline of Lake Bonneville. Quat. Sci. Rev. 159, 169–189. https://doi.org/10.1016/j.quascirev.2016.12.019.

Conway Morris, S., Robison, R.A., 1986. Middle Cambrian priapulids and other soft-bodied fossils from Utah and Spain, 117. University of Kansas, Paleontological Contributions, pp. 1–22.

Decrée, S., Herwartz, D., Mercadier, J., Miján, I., de Buffrénil, V., Leduc, T., Lambert, O., 2018. The post-mortem history of a bone revealed by its trace element signature: the case of a fossil whale rostrum. Chem. Geol. 477, 137–150. https://doi.org/10.1016/j.chemgeo.2017.12.021.

Deiss, C., 1938. Cambrian formations and sections in part of the Cordilleran Trough. Geol. Soc. Am. Bull. 49, 1067–1168. https://doi.org/10.1130/GSAB-49-1067.

Evans, J.P., Oaks Jr., R.Q., 1996. Three-dimensional variations in extensional fault shape and basin form: the Cache Valley basin, eastern Basin and Range province, United States. Geol. Soc. Am. Bull. 108, 1580–1593. https://doi.org/10.1130/0016-7606(1996)108<1580:TDVIEF>2.3.CO;2.

Gabbott, S.E., Hou, X.-G., Norry, M.J., Siveter, D.J., 2004. Preservation of early Cambrian animals of the Chengjiang biota. Geology 32, 901–904.

Gaines, R.R., 2014. Burgess Shale-type preservation and its distribution in space and time. In: Laflamme, M., Schiffbauer, J.D., Darroch, S.A.F. (Eds.), Reading and Writing of the Fossil Record: Preservational Pathways to Exceptional Fossilization. Paleontol. Soc. Pap, 20, pp. 123–146. https://doi.org/10.1017/S1089332600002837.

Gaines, R.R., Kennedy, M.J., Droser, M.L., 2005. A new hypothesis for organic preservation of Burgess Shale taxa in the middle Cambrian Wheeler Formation, House Range, Utah. Palaeogeogr. Palaeoclimatol. Palaeoecol. 220, 193–205. https://doi.org/10.1016/j.palaeo.2004.07.034.

Gaines, R.R., Briggs, D.E.G., Zhao, Y.L., 2008. Cambrian Burgess Shale-type deposits share a common mode of fossilization. Geology 36, 755–758. https://doi.org/10.1130/G24961A.1.

Gaines, R.R., Hammarlund, E.U., Hou, X., Qi, C., Gabbott, S.E., Zhao, Y., Peng, J., Canfield, D.E., 2012. Mechanism for Burgess Shale-type preservation. Proc. Natl. Acad. Sci. 109, 5180–5184. https://doi.org/10.1073/pnas.1111784109.

Gaines, R.R., Lombardo, A.J., Holzer, I.O., Caron, J.B., 2019. The limits of Burgess Shale-type preservation: Assessing the evidence for preservation of the blood protein hemocyanin in the Burgess Shale. Palaios 34, 291–299. https://doi.org/10.2110/palo.2019.026.

García-Bellido, D.C., Collins, D.H., 2006. A new study of *Marrella splendens* (Arthropoda, Marrellomorpha) from the Middle Cambrian Burgess Shale, British Columbia, Canada. Can. J. Earth Sci. 43, 721–742. https://doi.org/10.1139/e06-012.

Garson, D.E., Gaines, R.R., Droser, M.L., Liddell, W.D., Sappenfield, A., 2012. Dynamic palaeoredox and exceptional preservation in the Cambrian Spence Shale of Utah. Lethaia 45, 164–177. https://doi.org/10.1111/j.1502-3931.2011.00266.x.

Gueriau, P., Mocuta, C., Dutheil, D.B., Cohen, S.X., Thiaudière, D., Charbonnier, S., Clément, G., Bertrand, L., OT1 consortium, 2014. Trace elemental imaging of rare earth elements discriminates tissues at microscale in flat fossils. PLoS One 9, e86946. https://doi.org/10.1371/journal.pone.0086946.

Gutiérrez-Marco, J.C., García-Bellido, D.C., 2015. Micrometric detail in palaeoscolecid worms from late Ordovician sandstones of the Tafilalt Konservat-Lagerstätte, Morocco. Gondwana Res. 28, 875–881. https://doi.org/10.1016/j.gr.2014.04.006.

Harlov, D.E., Förster, H.J., 2003. Fluid-induced nucleation of (Y+ REE)-phosphate minerals within apatite: Nature and experiment. Part II. Fluorapatite. Am. Mineral. 88, 1209–1229. https://doi.org/10.2138/am-2003-8-905.

Herwartz, D., Tütken, T., Münker, C., Jochum, K.P., Stoll, B., Sander, P.M., 2011. Timescales and mechanisms of REE and Hf uptake in fossil bones. Geochim. Cosmochim. Acta 75, 82–105. https://doi.org/10.1016/j.gca.2010.09.036.

Herwartz, D., Tütken, T., Jochum, K.P., Sander, P.M., 2013. Rare earth element systematics of fossil bone revealed by LA-ICPMS analysis. Geochim. Cosmochim. Acta 103, 161–183. https://doi.org/10.1016/j.gca.2012.10.038.

Hylland, M.D., 2007. Surficial-geologic reconnaissance and scarp profiling on the Collinston and Clarkston Mountain Segments of the Wasatch Fault Zone, Box Elder County, Utah: Paleoseismic inferences, implications for adjacent segments, and issues for diffusion-equation scarp-age modeling. In: Lund, W.R. (Ed.), Paleoseismology of Utah, Utah Geological Survey Special Study 121, vol. 15. Utah Geological Survey, Salt Lake City, pp. 1–18.

Keenan, S.W., 2016. From bone to fossil: a review of the diagenesis of bioapatite. Am. Mineral. 101, 1943–1951. https://doi.org/10.2138/am-2016-5737.

Kimmig, J., Pratt, B.R., 2022. Evidence for microbially mediated silver enrichment in a middle Cambrian Burgess Shale-type deposit, Mackenzie Mountains, northwestern Canada. Can. J. Earth Sci. 59, 123–133. https://doi.org/10.1139/cjes-2021-0035.

Kimmig, J., Selden, P.A., 2021. A new shell-bearing organism from the Cambrian Spence Shale of Utah. Palaeoworld 30, 220–228. https://doi.org/10.1016/j.palwor.2020.05.003.

Kimmig, J., Strotz, L.C., Lieberman, B.S., 2017. The stalked filter feeder *Siphusauctum lloydguntheri* n. sp. from the middle Cambrian (Series 3, Stage 5) Spence Shale of Utah: its biological affinities and taphonomy. J. Paleontol. 91, 902–910. https://doi.org/10.1017/jpa.2017.57.

Kimmig, J., Strotz, L.C., Kimmig, S.R., Egenhoff, S.O., Lieberman, B.S., 2019. The Spence Shale Lagerstätte: an important window into Cambrian biodiversity. J. Geol. Soc. 176, 609–619. https://doi.org/10.1144/jgs2018-195.

Kloss, T.J., Dornbos, S.Q., Chen, J.Y., McHenry, L.J., Marenco, P.J., 2015. High-resolution geochemical evidence for oxic bottom waters in three Cambrian Burgess Shale-type deposits. Palaeogeogr. Palaeoclimatol. Palaeoecol. 440, 90–95. https://doi.org/10.1016/j.palaeo.2015.08.048.

Kocsis, L., Trueman, C.N., Palmer, M.R., 2010. Protracted diagenetic alteration of REE contents in fossil bioapatites: direct evidence from Lu–Hf isotope systematics. Geochim. Cosmochim. Acta 74, 6077–6092. https://doi.org/10.1016/j.gca.2010.08.007.

Kocsis, L., Botfalvai, G., Qamarina, Q., Razak, H., Király, E., Lugli, F., Wings, O., Lambertz, M., Raven, H., Briguglio, A., Rabi, M., 2020. Geochemical analyses suggest stratigraphic origin and late Miocene age of reworked vertebrate remains from Penanjong Beach in Brunei Darussalam (Borneo). Hist. Biol. 1–12 https://doi.org/10.1080/08912963.2020.1819999.

Legg, D.A., Pates, S., 2017. A restudy of *Utahcaris orion* (Euarthropoda) from the Spence Shale (middle Cambrian, Utah, USA). Geol. Mag. 154, 181–186. https://doi.org/10.1017/S0016756816000789.

Leibach, W.W., Lerosey-Aubril, R., Whitaker, A.F., Schiffbauer, J.D., Kimmig, J., 2021. First palaeoscolecid from the Cambrian (Drumian, Miaolingian) Marjum Formation of western Utah, USA. Acta Palaeontol. Pol. 66, 663–678.

Lerosey-Aubril, R., Hegna, T.A., Kier, C., Bonino, E., Habersetzer, J., Carré, M., 2012. Controls on gut phosphatisation: the trilobites from the Weeks Formation Lagerstätte (Cambrian; Utah). PLoS One 7, e32934. https://doi.org/10.1371/journal.pone.0032934.

Lerosey-Aubril, R., Gaines, R.R., Hegna, T.A., Ortega-Hernández, J., Van Roy, P., Kier, C., Bonino, E., 2018. The Weeks Formation Konservat-Lagerstätte and the evolutionary transition of Cambrian marine life. J. Geol. Soc. 175, 705–715. https://doi.org/10.1144/jgs2018-042.

Lerosey-Aubril, R., Kimmig, J., Pates, S., Skabelund, J., Weug, A., Ortega-Hernández, J., 2020. New exceptionally preserved panarthropods from the Drumian Wheeler Konservat-Lagerstätte of the House Range of Utah. Pap. Palaeontol. 6, 501–531. https://doi.org/10.1002/spp2.1307.

Liddell, W.D., Wright, S.H., Brett, C.E., 1997. Sequence stratigraphy and paleoecology of the Middle Cambrian Spence Shale in northern Utah and southern Idaho. Brigham Young Univ. Geol. Stud. 42, 59–78.

Lin, J.P., Briggs, D.E.G., 2010. Burgess Shale-type preservation: a comparison of naraoiids (Arthropoda) from three Cambrian localities. Palaios 25, 463–467. https://doi.org/10.2110/palo.2009.p09-145r.

LoDuca, S.T., Caron, J.B., Schiffbauer, J.D., Xiao, S., Kramer, A., 2015. A reexamination of Yuknessia from the Cambrian of British Columbia and Utah. J. Paleontol. 89, 82–95. https://doi.org/10.1017/jpa.2014.7.

MacFadden, B.J., Symister, C., Cannarozzi, N., Pimiento, C., De Gracia, C., 2015. Comparative diagenesis and rare earth element variation in Miocene invertebrate and vertebrate fossils from Panama. J. Geol. 123, 491–507. https://doi.org/10.1086/684006.

MacGabhann, B.A., 2012. A Solution to Darwin's Dilemma: Differential Taphonomy of Ediacaran and Palaeozoic Non-mineralised Discoidal Fossils (Doctoral Dissertation). National University of Ireland, Galway, p. 627.

Marshall, A.O., Wehrbein, R.L., Lieberman, B.S., Marshall, C.P., 2012. Raman spectroscopic investigations of Burgess Shale–type preservation: a new way forward. Palaios 27, 288–292. https://doi.org/10.2110/palo.2011.p11-041r.

Mayfield, D.B., Fairbrother, A., 2015. Examination of rare earth element concentration patterns in freshwater fish tissues. Chemosphere 120, 68–74. https://doi.org/10.1016/j.chemosphere.2014.06.010.

McCalpin, J., 1994. Neotectonic deformation along the East Cache fault zone, Cache County, Utah. In: Lund, W.R. (Ed.), Paleoseismology of Utah, Special Study 83, vol. 5. Utah Geological Survey, Salt Lake City, pp. 1–37.

Moon, J., Caron, J.B., Gaines, R.R., 2021. Synchrotron imagery of phosphatized eggs in *Waptia* cf. *W. fieldensis* from the middle Cambrian (Miaolingian; Wuliuan) Spence Shale of Utah. J. Paleontol. 1–12.

Moore, R.A., Lieberman, B.S., 2009. Preservation of early and middle Cambrian soft-bodied arthropods from the Pioche Shale, Nevada, USA. Palaeogeogr. Palaeoclimatol. Palaeoecol. 277, 57–62. https://doi.org/10.1016/j.palaeo.2009.02.014.

Nanglu, K., Caron, J.B., Gaines, R.R., 2020. The Burgess Shale paleocommunity with new insights from Marble Canyon, British Columbia. Paleobiology 46, 58–81. https://doi.org/10.1017/pab.2019.42.

Nielsen, M.L., Lee, M., Ng, H.C., Rushton, J.C., Hendry, K.R., Kihm, J.H., Nielsen, A.T., Park, T.Y.S., Vinther, J., Wilby, P.R., 2021. Metamorphism obscures primary taphonomic pathways in the early Cambrian Sirius Passet Lagerstätte, North Greenland. Geology. https://doi.org/10.1130/G48906.1.

Ou, Q., Vannier, J., Yang, X., Chen, A., Mai, H., Shu, D., Han, J., Fu, D., Wang, R., Mayer, G., 2020. Evolutionary trade-off in reproduction of Cambrian arthropods. Sci. Adv. 6, eaaz3376 https://doi.org/10.1126/sciadv.aaz3376.

Palmer, A.S., Snape, I., Stark, J.S., Johnstone, G.J., Townsend, A.T., 2006. Baseline metal concentrations in *Paramoera walkeri* from East Antarctica. Mar. Pollut. Bull. 52, 1441–1449. https://doi.org/10.1016/j.marpolbul.2006.04.012.

Pastorino, P., Bertoli, M., Squadrone, S., Brizio, P., Piazza, G., Noser, A.G.O., Prearo, M., Abete, M.C., Pizzul, E., 2019. Detection of trace elements in freshwater macrobenthic invertebrates of different functional feeding guilds: a case study in Northeast Italy. Ecohydrol. Hydrobiol. 19, 428–440. https://doi.org/10.1016/j.ecohyd.2019.04.006.

Pates, S., Daley, A.C., Lieberman, B.S., 2018. Hurdiid radiodontans from the middle Cambrian (Series 3) of Utah. J. Paleontol. 92, 99–113. https://doi.org/10.1017/jpa.2017.11.

Peel, J.S., Skovsted, C.B., Wallet, E., 2021. Morphology and ecology of the bradoriid arthropods *Spinospitella* and *Nikolarites* from the Cambrian (Series 2, stage 4) of North Greenland (Laurentia). Pal. Z. 95, 413–427.

Powell, W., 2003. Greenschist-facies metamorphism of the Burgess Shale and its implications for models of fossil formation and preservation. Can. J. Earth Sci. 40, 13–25. https://doi.org/10.1139/e02-103.

Pruss, S.B., Tosca, N.J., Stark, C., 2018. Small shelly fossil preservation and the role of early diagenetic redox in the early Triassic. Palaios 33, 441–450.

Pushie, M.J., Pratt, B.R., Pickering, I.J., George, G.N., MacDonald, T.C., 2014. Evidence for biogenic copper (hemocyanin) in the Middle Cambrian arthropod *Marrella* from the Burgess Shale. Palaios 29, 512–524. https://doi.org/10.2110/palo.2014.073.

Robison, R.A., 1991. Middle Cambrian biotic diversity: Examples from four Utah Lagerstätten. In: Simonetta, A.M., Conway-Morris, S. (Eds.), The Early Evolution of Metazoa and the Significance of Problematic Taxa. Cambridge University Press, Cambridge, pp. 77–98.

Robison, R.A., Babcock, L.E., Gunther, V.G., 2015. Exceptional Cambrian Fossils from Utah: A Window into the Age of Trilobites. Utah Geological Survey, Salt Lake City, p. 97.

Saleh, F., Antcliffe, J.B., Lefebvre, B., Pittet, B., Laibl, L., Peris, F.P., Lustri, L., Gueriau, P., Daley, A.C., 2020a. Taphonomic bias in exceptionally preserved biotas. Earth Planet. Sci. Lett. 529, 115873 https://doi.org/10.1016/j.epsl.2019.115873.

Saleh, F., Pittet, B., Sansjofre, P., Guériau, P., Lalonde, S., Perrillat, J.P., Vidal, M., Lucas, V., El Hariri, K., Kouraiss, K., Lefebvre, B., 2020b. Taphonomic pathway of exceptionally preserved fossils in the lower Ordovician of Morocco. Geobios 60, 99–115. https://doi.org/10.1016/j.geobios.2020.04.001.

Saleh, F., Vaucher, R., Antcliffe, J.B., Daley, A.C., El Hariri, K., Kouraiss, K., Lefebvre, B., Martin, E.L., Perrillat, J.P., Sansjofre, P., Vidal, M., 2021. Insights into soft-part preservation from the Early Ordovician Fezouata Biota. Earth-Sci. Rev. 103464 https://doi.org/10.1016/j.earscirev.2020.103464.

Schiffbauer, J.D., Wallace, A.F., Broce, J., Xiao, S., 2014. Exceptional fossil conservation through phosphatization. Paleontol. Soc. Pap. 20, 59–82. https://doi.org/10.1017/S1089332600002801.

Smith, M.R., 2014. Ontogeny, morphology and taxonomy of the soft-bodied Cambrian 'mollusc' *Wiwaxia*. Palaeontology 57, 215–229. https://doi.org/10.1111/pala.12063.

Strang, K.M., Armstrong, H.A., Harper, D.A.T., 2016. Minerals in the gut: scoping a Cambrian digestive system. R. Soc. Open Sci. 3, 160420 https://doi.org/10.1098/rsos.160420.

Streng, M., Ebbestad, J.O.R., Moczydłowska, M., 2008. A *Walcottella*-like bradoriid (Arthropoda) from the lower Cambrian of Sweden. GFF. 130, 11–19. https://doi.org/10.1080/11035890801301011.

Sundberg, F., 2020. Trilobite fauna (Wuliuan Stage, Miaolingian Series, Cambrian) of the lower Lakeview Limestone, Pend Oreille Lake, Idaho. J. Paleontol. 94, 1–49. https://doi.org/10.1017/jpa.2020.38.

Tian, L., Jie, Y., Jin-Bo, H., Xi-Guang, Z., 2015. The feeding behaviour of the Cambrian tubiculous priapulid *Selkirkia*. Lethaia 48, 125–132. https://doi.org/10.1111/let.12093.

Valenti, G.L., 1982. Structure of the Laketown Quadrangle and petroleum exploration in the Bear Lake area, Rich County, Utah. In: Powers, R.B. (Ed.), Geologic Studies of the Cordilleran Thrust Belt, Vol. 2. Rocky Mountain Association of Geologists, Denver, pp. 859–868.

Vannier, J., Chen, J., 2005. Early Cambrian food chain: new evidence from fossil aggregates in the Maotianshan Shale biota, SW China. Palaios 20, 3–26. https://doi.org/10.2110/palo.2003.p03-40.

Vannier, J., Williams, M., Alvaro, J.J., Vizcaïno, D., Monceret, S., Monceret, E., 2005. New early Cambrian bivalved arthropods from southern France. Geol. Mag. 142, 751–763. https://doi.org/10.1017/S0016756805001093.

Vannier, J., Liu, J., Lerosey-Aubril, R., Vinther, J., Daley, A.C., 2014. Sophisticated digestive systems in early arthropods. Nat. Commun. 5, 1–9. https://doi.org/10.1038/ncomms4641.

Walcott, C.D., 1908. Nomenclature of some Cambrian Cordilleran Formations. In: Cambrian Geology and Paleontology, Smith. Misc Collns, 53, pp. 1–12.

Wang, D., Vannier, J., Aria, C., Sun, J., Han, J., 2021. Tube-dwelling in early animals exemplified by Cambrian scalidophoran worms. BMC Biol. 19, 1–20. https://doi.org/10.1186/s12915-021-01172-4.

Wen, R., Babcock, L.E., Peng, J., Robison, R.A., 2019. New edrioasteroid (Echinodermata) from the Spence Shale (Cambrian), Idaho, USA: further evidence of attachment in the early evolutionary history of edrioasteroids. Bull. Geosci. 94, 115–124. https://doi.org/10.3140/bull.geosci.1730.

Whitaker, A.F., Kimmig, J., 2020. Anthropologically introduced biases in natural history collections, with a case study on the invertebrate paleontology collections from the middle Cambrian Spence Shale Lagerstätte. Palaeontol. Electron. 23, a58 https://doi.org/10.26879/1106.

Whitaker, A.F., Jamison, P.G., Schiffbauer, J.D., Kimmig, J., 2020. Re-description of the Spence Shale palaeoscolecids in light of new morphological features with comments on palaeoscolecid taxonomy and taphonomy. Pal. Z. 94, 661–674. https://doi.org/10.1007/s12542-020-00516-9.

Williams, J.S., 1948. Geology of the Paleozoic rocks, Logan quadrangle, Utah. Geol. Soc. Am. Bull. 59, 1121–1164.

Yang, X., Kimmig, J., Zhai, D., Liu, Y., Kimmig, S.R., Peng, S., 2021a. A juvenile-rich palaeocommunity of the lower Cambrian Chengjiang sheds light on palaeo-boom or palaeo-bust environments. Nat. Ecol. Evol. 5, 1082–1090. https://doi.org/10.1038/s41559-021-01490-4.

Yang, X.-Y., Vannier, J., Yang, J., Wang, D., Zhang, X.G., 2021b. Priapulid worms from the Cambrian of China shed light on reproduction in early animals. Geosci. Front. 12, 101234 https://doi.org/10.1016/j.gsf.2021.101234.

Zacaï, A., Vannier, J., Lerosey-Aubril, R., 2016. Reconstructing the diet of a 505-million-year-old arthropod: *Sidneyia inexpectans* from the Burgess Shale fauna. Arth. Struct. Devel. 45, 200–220. https://doi.org/10.1016/j.asd.2015.09.003.

Zhang, L., Algeo, T.J., Cao, L., Zhao, L., Chen, Z.Q., Li, Z., 2016. Diagenetic uptake of rare earth elements by conodont apatite. Palaeogeogr. Palaeoclimatol. Palaeoecol. 458, 176–197. https://doi.org/10.1016/j.palaeo.2015.10.049.

Zhu, M.Y., Vannier, J., Iten, H.V., Zhao, Y.L., 2004. Direct evidence for predation on trilobites in the Cambrian. Proc. R. Soc. Lond. B 271, S277–S280. https://doi.org/10.1098/rsbl.2004.0194.

Zhu, M., Babcock, L.E., Steiner, M., 2005. Fossilization modes in the Chengjiang Lagerstätte (Cambrian of China): testing the roles of organic preservation and diagenetic alteration in exceptional preservation. Palaeogeogr. Palaeoclimatol. Palaeoecol. 220, 31–46. https://doi.org/10.1016/j.palaeo.2003.03.001.